

1 Research Article

2 **Stratigraphic modeling of the Western Taiwan foreland**
3 **basin: sediment flux from a growing mountain range**
4 **and tectonic implications**

5 Stefan Nagel ^a, Didier Granjeon ^b, Sean Willett ^a, Andrew Tien-Shun Lin ^c,
6 Sébastien Castellort ^{a,d,*}

7 ^a *Department of Earth Sciences, ETH Zürich, Sonneggstrasse 5, 8092 Zürich, Switzerland*

8 ^b *IFP Energies Nouvelles, Rueil-Malmaison, Paris, France*

9 ^c *Department of Earth Sciences, National Central University, 300 Jungha Road, Chungli, Taoyuan 101, Taiwan*

10 ^d *Department of Earth Sciences, University of Geneva, Rue des Maraichers 13, 1205 Geneva, Switzerland*

11
12 *Keywords*

13 Taiwan

14 Foreland basin

15 Tectonic sedimentology

16 Arc-continent collision

17 Stratigraphic modeling

18 Erosion

19 Sedimentation

20

21 **ABSTRACT**

22 Sediment flux signals from source to sink in foreland basins preserve a record of tectonics, sea level
23 and climate through erosion and sedimentation. However, longitudinal sediment transport often occurs
24 in foreland basins, thus removing part of the orogenic material flux from foreland basin records. Here
25 we use mass balance calculation and stratigraphic simulations of sediment fluxes for the Taiwan
26 orogen to provide an order of magnitude estimate of how much orogenic material may bypass a
27 foreland basin. Our results indicate a significant, potentially more than 50%, mismatch between
28 sediment volume currently preserved in the basin and the amount of material presumably eroded from
29 the orogen since the onset of collision in Taiwan. This suggests either a significant overestimation of
30 average erosion rates over the period concerned with orogenic development of Taiwan, or it supports
31 previous paleogeographic work suggesting that longitudinal sediment transport in the paleo-Taiwan
32 Strait served as a major bypass conduit of importance for the establishment of a steady state orogen.
33 We identify candidate submarine topography in the South China Sea that may preserve Taiwan's
34 missing erosional mass.

35

36 **1. Introduction**

37 Sediment fluxes within foreland basins exert a primary control on basin architecture involving
38 interactions between tectonics, sea level and climate through erosion and sedimentation (e.g., Allen et
39 al., 2013, Castellort et al., 2015, Flemings and Jordan, 1989, Posamentier and Allen, 1993). The
40 orogenic history of many ancient basins has been reconstructed with help of sedimentary records, such

* Corresponding author. Tel: +41 223796616
E-mail address: sebastien.castellort@unige.ch (S. Castellort)

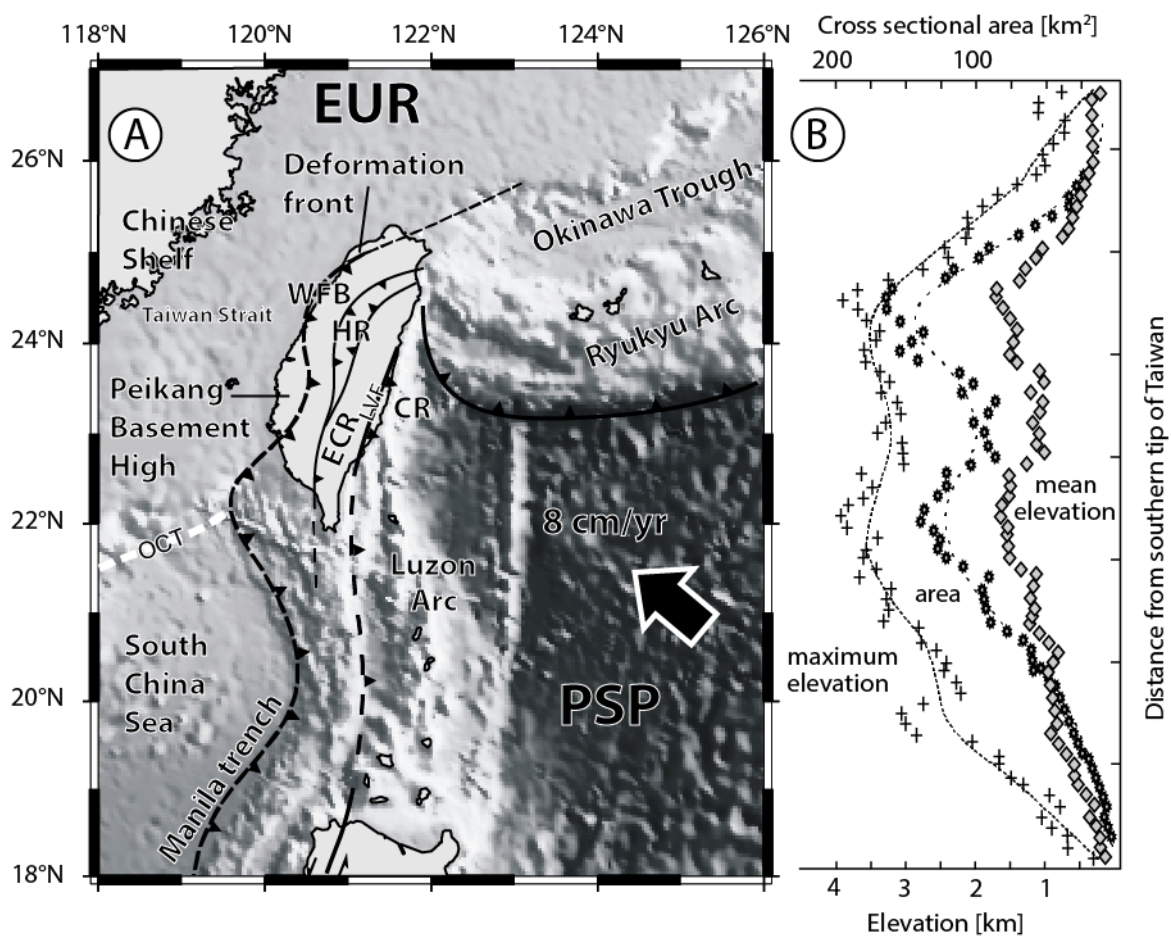
41 as in the Alps (Garzanti et al., 2004; Lihou and Allen, 1996), Pyrenees (Puigdefàbregas et al., 1992;
42 Vergés and Burbank, 1996), or Himalayas (Garzanti et al., 2005; White et al., 2002), but it is still not
43 well known how much of the orogenic history is eventually preserved and how tectonics, facies and
44 sediment supply to basins are linked (Castelltort et al., 2015, Romans et al., 2016).

45 The western foreland basin in Taiwan (Fig. 1A) is a particularly suitable place to study interactions
46 between tectonics and sediment fluxes because it is very young (5-6 Ma) and still very active (modern
47 seismicity and extreme climate conditions). In this basin, southwestward ongoing oblique collision
48 between the Luzon volcanic arc and the continental shelf of Eurasia (OCT: Ocean-Continent
49 Transition on figure 1A) makes it possible to record the full evolution of basin deformation (e.g.,
50 Suppe, 1981, Covey, 1984, Lin et al., 2003) and provides an opportunity to connect tectonics and
51 depositional processes at different stages of the basin's evolution. The western foreland of Taiwan is
52 the historical basin where the classical foreland filling sequence was first described by Covey (1984,
53 1986). Indeed, the basin evolved from an early underfilled stage with relatively deep-water
54 sedimentation (now observable in the modern setting in the South of the orogen) to a late balanced-
55 filled stage, where shallow marine environments persist until today (most of modern Taiwan Strait,
56 Covey, 1984), despite the enormous amount of sediment supplied to the ocean by the rising Taiwan
57 mountains (Milliman and Kao, 2005; Milliman and Syvitski, 1992). In that sense, Taiwan orogen is
58 emblematic of the distinct classical evolutionary stages (underfill to overfill, flysch to molasse) that
59 characterize many ancient foreland basin systems such as in the Molasse basin of the Alps (Allen et
60 al., 1991), the Bradanic Trough in the Apennines (Tropeano et al., 2002), the Solomon Sea in Papua
61 New Guinea (Silver et al., 1991) or the South-Pyrenean foreland basin (Puigdefàbregas and Souquet,
62 1986). As a consequence of oblique collision, the basin records a time-transgressive southwestward
63 oriented migration of facies belts (e.g., Covey, 1984, Chen et al., 2001, Nagel et al., 2013) and
64 sediment depocenters (Simoes and Avouac, 2006), similar to other oblique collisions such as in Papua
65 New Guinea (Abbott et al., 1994; Silver et al., 1991), but the details of the geometry of the initial
66 collision at the scale of Taiwan are still ambiguous and several models have been proposed. Whereas
67 some models favor an arc-continent collision (Huang et al., 2006; Suppe, 1984, 1988; Teng, 1990),
68 others suggested a two stage collision of an exotic block with the Eurasian continental margin and a
69 second collision of Luzon volcanic arc with the passive margin (Lu and Hsü, 1992), or an arc-arc
70 collision between Luzon volcanic arc and a paleo-Ryukyu arc system extending to the west of Taiwan
71 (Seno and Kawanishi, 2009; Sibuet and Hsu, 1997; Sibuet et al., 1995), or even that collision may
72 have happened synchronously along the margin at the scale of Taiwan (within a larger scale context of
73 obliquity between EUR and PSP, Fig. 1A, Castelltort et al., 2011; Lee et al., 2015).

74 From an orogenic point of view, Taiwan has been proposed as a possible illustration of topographic
75 steady state in a critical orogenic wedge because it shows an approximately constant width of 90 km
76 (Suppe, 1981, Stolar et al., 2007) and elevations and cross-sectional area plateau in the central segment
77 of the belt (Fig. 1B). Indeed, were it not at steady state, the orogen should be wider in the North were
78 collision started earlier, and progressively narrower southwards. Instead the cylindrical shape of the
79 orogen suggests that it has reached a critical size and slope. As a consequence, Taiwan orogen has
80 been taken as an emblematic example of a steady state orogen in which erosional processes are able to
81 balance uplift rates. As a note of caution, we remark that some authors have explained that the idea of
82 steady state applies at large-scale in Taiwan but that, most probably, the high-frequency climate
83 oscillations linked to orbital climate shifts, prevent the establishment of pure steady state at all scales
84 (e.g., Whipple, 2001). Additionally, the Western foredeep itself also eventually reached a steady state
85 size where accommodation space stayed constant despite the large sediment fluxes from Taiwan
86 mountains (Covey, 1984; Covey, 1986). Therefore Covey (1986) suggested that sediment bypass out
87 of the basin must have been an important factor that balanced accommodation space and sediment

88 supply, maintaining the basin shallow marine, and preventing it from becoming overfilled or even
 89 fully terrestrial.

90 The aim of this paper is to test, within the frame given by tectonic (plate boundaries configuration and
 91 timing, basin evolution) and geomorphic (steady state, erosion and sediment supply rates) constraints
 92 exposed above, the plausibility and magnitude of sediment bypass and to discuss implications for
 93 understanding foreland basins architecture within a well constrained source-to-sink setting. To do this,
 94 we use 3D stratigraphic simulations with different tectonic scenarios and we try to compare them with
 95 seismic lines from the Taiwan Strait to evaluate the match between simulations and observations.
 96 These simulations show how different tectonic settings control the stratigraphic evolution of the
 97 foreland basin, and allow to quantify sediment budget for the source-to-sink system. Results
 98 emphasize a significant mismatch between preserved volumes in the foreland with respect to volumes
 99 predicted given inferred erosion rates and topographic development. We discuss the implications of
 100 these contradictions for the importance of longitudinal sediment transport in foreland basins.
 101



102
 103 Figure 1. Geodynamic context of the collision in Taiwan and along-strike morphology. A) The plate context and main
 104 structural units in Taiwan. Note the overall obliquity between the Luzon Arc - Manila Trench system and the Eurasian
 105 margin (OCT). PSP: Philippine Sea Plate; EUR: Eurasian Plate; WF: western Foothills; HR: Hsüehshan Range; ECR:
 106 Eastern Central Range; LVF: Longitudinal Valley Fault; CR: Coastal Range; OCT: Ocean-Continent Transition. B)
 107 Longitudinal evolution of maximum elevation, mean elevation and cross-sectional area of the orogen (after Stolar et al.,
 108 2007, Suppe, 1981). The "plateau" of all three parameters displayed by the central segment of the orogen suggests that the
 109 mountain belt has reached a constant size and height despite the longer collisional history in the North compared to the
 110 South. Based on this assumption, Suppe (1981) among others have suggested that the orogen is at steady state, i.e. has
 111 reached a critical size for which tectonic influx of material is in overall balance with erosion. Decreasing elevation in the
 112 North is due to mountain range collapse associated with propagation of the extensional regime of the Okinawa Through. In
 113 the South, the orogen is still growing, has not reached steady state, hence the tapering elevation and decreasing width.

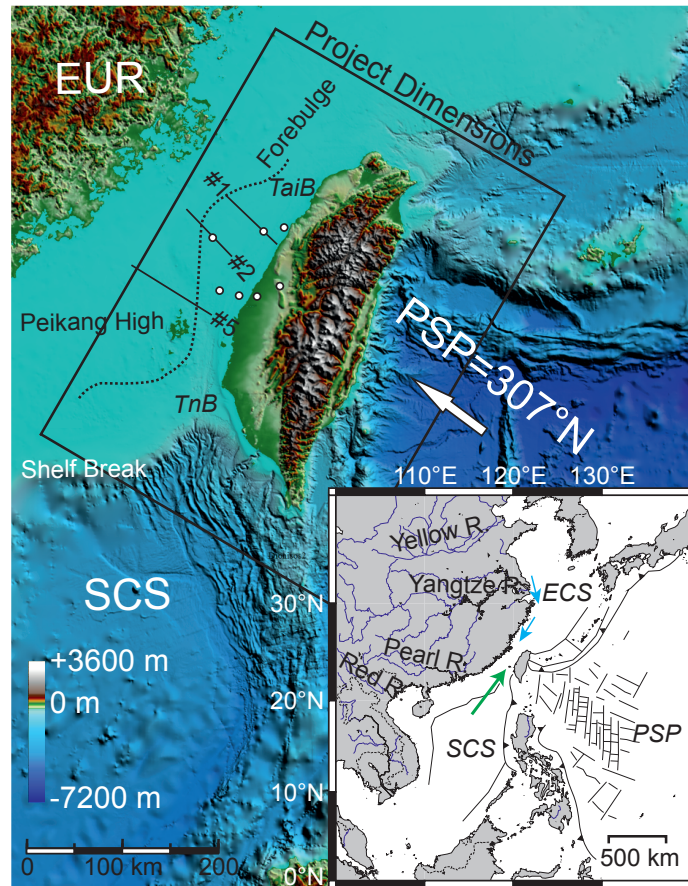
115

116 **2. General setting and background**117 *2.1. Geology and Tectonics*

118 The Taiwan mountains, rising almost 4 km above sea level, formed by collision between Philippine
119 Sea plate and Eurasian continent shelf (Fig. 1A, Fig. 2). Arc volcanism associated with subduction
120 below the Philippine sea plate ceased between 6 Ma and 3 Ma, when the arc resisted subduction and
121 collided with the Asian passive margin to form an initial accretionary wedge (Huang et al., 2006;
122 Yang et al., 1995). In most recent studies, arc-continent collision is estimated to have initiated in late
123 Pliocene (Nagel et al., 2013; see discussion below). This is based on observing a continuous sandstone
124 provenance shift and increasing illite crystallinity, interpreted to represent progressive unroofing and
125 recycling of the metamorphic orogenic belt (Dorsey and Lundberg, 1988; Nagel et al., 2013). Oblique
126 collision between the N-S trending Luzon volcanic arc and the NE-SW trending passive margin
127 resulted in southwest propagating collision (e.g., Nagel et al., 2013; Simoes and Avouac, 2006; Suppe,
128 1981; Teng, 1990), with modern collision point presently located offshore SW Taiwan (Lin et al.,
129 2008; Yu and Huang, 2009). Today, the southernmost tip of Taiwan, which exhibits transient
130 landscape features (Giletecz et al., 2015), represents the youngest relief associated with the emerging
131 orogen. Oceanic lithosphere in the South China Sea is currently being subducted below the Philippine
132 sea plate along the Manila Trench (Fig. 1A) whereas the Philippine sea plate itself is being subducted
133 northwards below the Eurasian plate (Kao et al., 2000). This complex plate interaction manifests high
134 active seismicity associated with a convergence rate of 70-80 km/Ma between the Philippine sea plate
135 and the Eurasian continent (Seno et al., 1993; Wu et al., 2009; Wu et al., 2007; Yu et al., 1997). The
136 current plate convergence is mainly accommodated within the Longitudinal Valley Fault (LVF, Fig.
137 1A) on the east coast and at the deformation front in the Western Foothills consistent with the main
138 active faults (Yu et al., 1997).

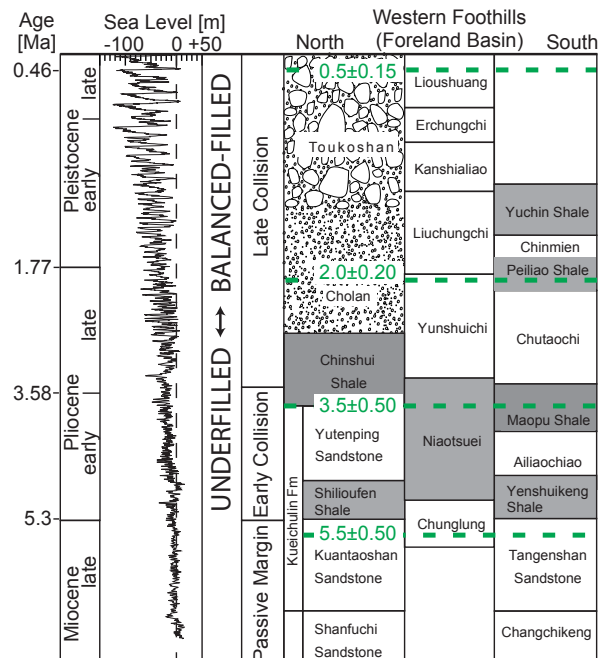
139 The continental margin experienced extensive rifting and continental breakup phases due to the
140 opening of the South China Sea in late Paleogene, which resulted in major subsidence and numerous
141 sub-basins separated by topographic highs (Lee and Lawver, 1995; Lin et al., 2003). This pre-
142 collisional segmentation of the margin has an influence on the current structuration of the orogen into
143 different tectonic units (Fig. 1A, Fig. 4B) that consist of (1) accreted volcanic arc (CR: Coastal Range)
144 separated by suture zone (LVF: Longitudinal Valley Fault), (2) main orogenic belt (ECR: Eastern
145 Central Range), (3) Hsuechan Range (HR), (4) deformed and uplifted foreland basin strata which
146 constitutes a classical foreland with a fold-and-thrust belt (Western Foreland Basin), and (5)
147 undeformed onshore (Coastal Plain) and offshore foreland basin sediments (Ho, 1988).

148



149
 150 **Figure 2:** Bathymetric and plate tectonic framework of the studied area showing boundaries of stratigraphic model. Inset
 151 shows large-scale plate setting. Seismic lines tracks are from Yu and Chou (2001). Inset shows the four major Chinese river
 152 systems in the area of Taiwan. Large green arrow is South China Sea Current (northward), and small blue arrows are China
 153 Coastal Currents (southward). EUR: Eurasia. ECS: East China Sea. PSP: Philippines Sea Plate. SCS: South China Sea. TaiB:
 154 Taishi Basin. TnB: Tainan Basin.

155
 156 As initially described by Covey (1984), the evolution of syn-collisional facies is very similar from
 157 north to south, except for distinctive grain size contrasts (Chou, 1973). The coarse fraction was
 158 trapped in a shallow continental shelf basin (Taishi Basin, TaiB on Fig. 2), which was separated from
 159 the South by the Peikang High topographic barrier (Fig. 1A and Fig. 2, Meng, 1967). Most of fine
 160 grain sizes were transported further southwards and became deposited in a deep marine basin to the
 161 South (Tainan Basin and/or South China Sea, TnB on Fig. 2).



162

163 **Figure 3:** Schematic stratigraphy of the foreland basin of Taiwan from north to south. Note the change in lithology in Central
164 and South-Taiwan due to the topographic barrier called Peikang High, which separated the northern Taishi basin and the
165 southern Tainan basin (see location on Fig. 2). Thick Conglomeratic units up to 3'000 m are found in the Toukoshan fm.,
166 which is made of coarse alluvial and fluvial sediments. The sea level curve is adapted from Miller et al. (2011). The key
167 dated horizons (Nannofossils, see synthesis in Nagel et al., 2013) are marked with thick dashed lines. Shales are in grey.
168 Sandstones or sandstones and shales are in white. The Cholan formation is particularly coarse-grained, and the Toukoshan
169 formation is conglomeratic.

170

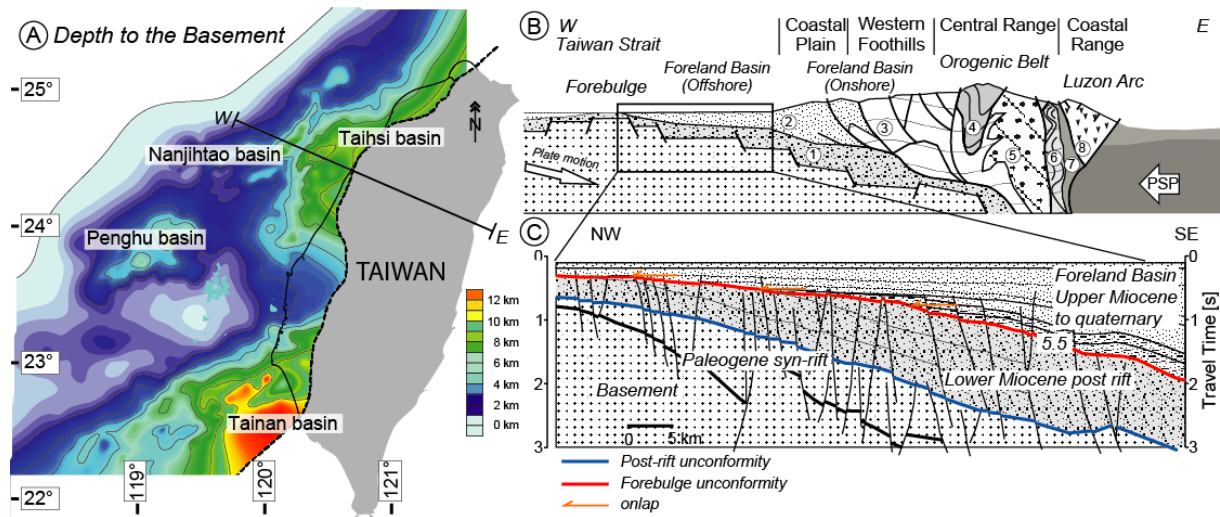
171 The chronostratigraphy of the Western Foothills has been extensively studied with Neogene
172 calcareous nannofossils (Chang and Chi, 1983; Chou, 1973; Huang, 1977; Huang and Huang, 1984)
173 and provides ground truth for five key biostratigraphic horizons (the most recent four are on figure 3)
174 that are best documented (see synthesis in Nagel et al., 2013): nannofossil zone boundaries NN5-6
175 ($12.5\pm 1\text{Ma}$), NN11-12 ($5.5\pm 0.5\text{Ma}$), NN15-16 ($3.5\pm 0.5\text{Ma}$), NN18-19 ($2\pm 0.2\text{Ma}$) and NN19-20
176 ($0.5\pm 0.15\text{Ma}$). The stratigraphic succession comprises a first retrogradational series consisting of
177 shallow marine deltaic environments, which are often tidally influenced (Fig. 3, Kueichulin fm.). The
178 transgression associated with the end of this formation marks the onset of orogenic loading of the
179 shallow marine shelf environment. To the South, the formation passes progressively into deeper
180 marine mud-dominated deposits (Fig. 3). The source of sediments during deposition of Kueichulin
181 formation is essentially the same as during previous passive margin history of the basin, from the
182 Eurasian continent to the southeast (Castelltort et al., 2011; Nagel et al., 2013; Shaw, 1996). It is
183 followed by the Pliocene Chinshui Shale, a relatively deep marine mud-dominated formation, which
184 represents the underfilled stage of the foreland basin (Covey, 1984). Reworked fossils, paleocurrent
185 directions and facies analysis point to a main source from the East of the basin at this period, which is
186 the growing orogenic wedge (Chang and Chi, 1983; Nagel, 2012; Nagel et al., 2013). The Cholan
187 formation represents a large-scale progradational sequence of shallow marine wave- and tide-
188 influenced environments, which became progressively dominated by fluvial processes upsection. This
189 is the main foreland basin stage driven by large sediment fluxes out of Taiwan orogen and southward
190 migration of facies belts. During late Pleistocene, increased erosion lead to deposition of large alluvial
191 sediments, which most likely are an ancient example of braided rivers draining the orogen today
192 (Covey, 1984).

193

194 2.2. The foreland basin unconformity

195 Flexural response due to loading of the Eurasian shelf by the forming orogen and its sedimentary
196 response has been studied in detail (Castelltort et al., 2011; Chen et al., 2001a; Chiang et al., 2004;
197 Simoes and Avouac, 2006; Tensi et al., 2006). Tensi et al. (2006) suggested that the passive margin
198 lithosphere already experienced flexure since 12.5 Ma and interpreted the observed flexure as not
199 being related to initial arc-continent collision, which is consistent with plate kinematic reconstructions
200 (Hall, 1996; Nagel et al., in prep; Sibuet and Hsu, 2004). The basal foreland unconformity is observed
201 in the Northern basins (Taishi basin, Fig. 4) with an age estimated between 8.6 and 5.6 Ma (based on
202 biostratigraphic data), consistent with a flexural migration of the load from east to west (Lin and
203 Watts, 2002; Lin et al., 2003). This unconformity separates the passive margin sequence and the
204 foreland basin sequence, which onlaps onto it. The depositional hiatus increases in duration from the
205 current frontal thrust towards the forebulge in the middle of Taiwan Strait (Lin et al., 2003; Yu and
206 Chou, 2001).

207



208
209

210 **Figure 4:** A) Map of depth to the Cenozoic basement in Taiwan's foreland, highlighting four individual basins separated by
 211 basement highs. The Nanjihtao basin is partially covered by a distal foreland basin sequence. The Taihsi and Tainan basin are
 212 separated by the Peikang High. Figure modified from Lin and Watts (2003). B) Schematic cross-section of the Taiwan
 213 orogen in the North, where the interpreted forebulge topography is most pronounced. 1) Lower Miocene post-rift sequence,
 214 2) Upper Miocene to quaternary foreland sequence, 3) Miocene to Pleistocene sequences of the Western Foothills, 4) Eocene
 215 to Miocene metapelites, 5) and 6) Metamorphic formations of the Tananao Complex, 7) Neogenes sandstones and
 216 conglomerates, 8) Volcanic rocks and volcanoclastic of the Coastal Ranges (Luzon Arc). C) Detailed seismic line drawing
 217 modified from Yu and Chou (2001). The foreland basin sequence onlaps onto passive margin deposits, with increasing
 218 depositional hiatus towards the forebulge, where late Pleistocene-Quaternary sediments directly overlie lower Miocene strata.
 219

220 2.3. Modern sediment fluxes in Taiwan: uplift, climate and erosion

221 East Asian monsoonal climate was most probably established since 8.5 Ma (i.e., late Miocene) with an
 222 intensification observed since 5 to 3 Ma (Liu et al., 2003; Wan et al., 2006; Zheng et al., 2004). Today
 223 the island experiences 4 to 6 typhoons per year, with maximum mean annual rainfall of 2000-3000
 224 mm yr⁻¹ (Kao and Milliman, 2008). The total annual amount of sediment delivered to the ocean by
 225 Taiwanese rivers has been estimated to be up to 500 Mtyr⁻¹ with a strong asymmetry across the
 226 mountain range (Dadson et al., 2003; Liu et al., 2008). Estimates of erosion rates range between 2.2 to
 227 8.3 mmyr⁻¹ (Dadson et al., 2003; Fuller et al., 2003) and up to 30 mmyr⁻¹ (Resentini et al., 2017) in
 228 agreement with quantitative estimates from thermochronometric constraints of 3 to 10 mmyr⁻¹ (Lee et
 229 al., 2006; Willett et al., 2003).

230 Much of the suspended sediment is delivered at hyperpycnal concentrations into the Taiwan Strait
 231 (Dadson et al., 2005; Milliman and Kao, 2005; Milliman et al., 2007) where it is redistributed by
 232 seasonal and tidal currents (Jan et al., 2002). The northeast directed South China Sea current (green
 233 arrow, inset Fig. 2), for example, transports warm tropical water into the Strait with a peak intensity
 234 during summer months (June to August). In contrast, the southwest directed China Coastal current
 235 (blue arrows, Fig. 2) delivers Yangtze-derived mud into the northern Taiwan Strait (Hu et al., 2010;
 236 Xu et al., 2009) during winter months (September to May).

237 Marine observations indicate that fine mud particles are relatively quickly transported northwards out
 238 of the Taiwan Strait (Horng and Huh, 2011; Horng et al., 2012; Huh et al., 2011; Kao et al., 2008a;
 239 Liu et al., 2010; Milliman et al., 2007). For example, marine investigations in the Choshui river delta
 240 made before and after a typhoon hit the island, showed that fine-size particles are redistributed and
 241 transported northward within a month (Milliman et al., 2007). Thus, sediments eroded from the orogen
 242 possibly contained a larger amount of mud than currently found in ancient plio-pleistocene deposits,
 243 and that has been fractionated away by marine processes.

244 Average sedimentation rates vary greatly from 2 mm yr⁻¹ in the Western foreland basin to 3-4 mm yr⁻¹
 245 in the Coastal Range (Chen et al., 2001a; Lin et al., 2003; Lundberg and Dorsey, 1990), with a rapid
 246 increase observed since the onset of deformation in the Western Foothills (Chang et al., 1983; Lock,
 247 2007; Mouthereau and Lacombe, 2006; Mouthereau et al., 2001). These values are in accordance with
 248 erosion rates estimates of between 2 and 10 mm yr⁻¹ from modern river sediment loads and
 249 interpretation of thermochronological data (Dadson et al., 2003; Fuller et al., 2003; Fuller et al., 2006;
 250 Liu et al., 2001; Liu et al., 2000; Siame et al., 2011; Simoes et al., 2007; Simoes and Avouac, 2006;
 251 Willett et al., 2003)(Table 1).

Author/Year	Uplift (U)/Exhumation Rate (E) [mm/a]	Erosion Rate/Incision Rate (I) [mm/a]
Peng et al. (1977)	U: 5±0.7 (<9 ka) Holocene coral reefs ¹	
Liu (1982)	U: 4.2-6.8 (3-0.5 Ma) 8.9±1.9 (<0.6 Ma)	
Jahn et al. (1986)	U: 3-4 (<3 Ma) Rb-Sr isotopes (TC)	
Lundberg and Dorsey (1990)	U: 5.9-7.5 (<1.3-0.9 Ma) CoR	6-7 (<1 Ma)
Wang and Burnett (1990)	U: 1.2-6.1 10 ka (Holocene) ²	
Chen et al. (1991)	U: 5-14 (<5000 a) (CoR, uplifted corals)	
Liew et al. (1993)	U: 2.5-8 (Holocene) elevated shoreline deposits (CoR)	
Lo and Onstott (1995)	E: 1.7-1.6 (K-Ar reset ages)	
Liu (1995)	U: 36-42 (<10a, GPS, CR)	
Liu et al. (2000, 2001)		2.5-4.6 (<4 Ma) 2.3-6 (TC) ZFT/AFT
Hsieh and Knuepfer (2002)	U: <10 (Holocene river terrace)	I: <20 (river incision)
Dadson et al. (2003)	E: 3-6 (ECR) 1.5-2.5 (SW Taiwan)	5.2 (<30a) SSC ³ 6 (CR), up to 60 ⁴ I: 1.5-9 (Holocene)
Fuller et al. (2003)		2.2-8.3 (8-27a, SSC)
Willett et al. (2003)		7-8 4-6 (AFT/ZFT)
Yamaguchi and Ota (2004)	U: 5-15 (<13 ka) Holocene marine terraces (CoR)	
Song et al. (2004)	U: 10.9, 5.4 Holocene marine terraces (CoR)	
Simoes and Avouac (2006); Simoes et al. (2007b,a) ⁵		4.2 (BR)-6.3 (TC) 2-3 (<1.5 Ma)
Fuller et al. (2006)	E: 3-5 (acceleration since 2-1 Ma)	2.3-3.3 (AFT/ZFT ⁶) max. 6 - 8
Lee et al. (2006)	U: <1 (6-1 Ma) 4-10 (<1 Ma)	
Siame et al. (2011)		2 ±1 (<100 ka), 5-7 (<50 a) ⁷
Kuo-En (2011)	U: 0.2-18.5 (2000-2008, GPS) (BR)	
Siame et al. (2012)		I: 0.8±0.1 - 10.1±1.3 (<300 ka) (Choshui river terraces)

¹Hengchun Peninsula, Tainan area, Coastal Range

²Hengchun Peninsula, Coastal Range, Lanyu and Lutao

³SSC=calculation based on modern suspended sediment concentrations

⁴active thrust faults, Western Foothills, Southwest Taiwan

⁵thermokinematic modeling

⁶BR=Backbone Range, TC=Tananao complex, CR=Central Range, ECR=Eastern Central Range, CoR=Coastal Range

⁷Be10, Lanyang catchment

252

253

Table 1: Synthesis of observed and predicted uplift and erosion rate data for the Taiwan orogen.

254

255 3. Material and methods

256 As explained in introduction, the aim of this paper is to test the influence of different tectonomorphic
 257 scenarios in controlling the stratigraphic architecture of the Western Foreland Basin of Taiwan, with a
 258 focus on constraining the magnitude of sediment bypass out of the basin and its implications for
 259 understanding the underfill to overfill evolution of foreland basins.

260 To do this we use a stratigraphic model that requires two main input conditions: subsidence/uplift and
 261 sediment fluxes. In the following sections, we introduce the basic physical laws used in the 3D
 262 stratigraphic model Dionisos and we then review the data and processing that are behind subsidence
 263 and sediment flux patterns that we use in this work and that are based on observations reviewed in the
 264 previous geological setting section. Finally, we outline the setup of numerical experiments.

265 3.1. 3D stratigraphic model "Dionisos"

266 To evaluate the complex relationships between the stratigraphic record, tectonics (subsidence, with
 267 respect to the initial collisional geometry) and climate (erosion rates), the stratigraphic model Dionisos
 268 was used (Granjeon, 1997). Dionisos is a process-based modelling tool using a diffusion and advection
 269 law that links sediment flux to local slope (potential available energy to move sediment) and water
 270 flow (transport efficiency of the lithologies defined) by a diffusion coefficient. Erosion and
 271 sedimentation at each point of the basin are defined by combining the transport equation and the law
 272 of mass conservation:

$$Q_{sed} = -K \cdot Q_{water} \cdot \overrightarrow{grad} h$$

273 The second basic assumption of the model is the law of mass conservation

$$\frac{\partial h}{\partial t} = -div Q_{sed}$$

274 where:

275 Q_{sed} = sediment transport [m^2/s]

276 Q_{water} = relative water flow [-]

277 K = diffusion coefficient [m^2/yr]

278 h = ground elevation [m]

279 $\delta h/\delta x$ = elevation gradient (i.e., slope)

280 Boundary supplies (i.e. sediment volume and sand, mud fraction), water discharge of rivers at source
 281 locations and rainfall must be defined for each sedimentary sequence. It is important to note that all
 282 the water introduced by rivers and rainfall is conserved and flows towards the lowest part of the basin
 283 (Granjeon and Joseph, 1999). The potential sediment availability is simulated by a maximum erosion
 284 rate, which depends on climate (rainfall), subsidence rate and uplift rate (topographic elevation).

285 The study area was set as a 500 km x 320 km rectangle in the Taiwan Strait where abundant data is
 286 available (Fig. 2). It is confined to the flexural forebulge in the West and to the Coastal Range in the
 287 East, and includes the Taishi basin in the North and the Tainan Basin in the South (Fig. 2). The input
 288 data required by Dionisos consist of tectonic subsidence for different time intervals, sediment supply
 289 and eustatic sea level fluctuations. Parameters for compaction, flexure and sediment transport are
 290 embedded within the model and can be adjusted to fit benchmark geological data. Sediment influx can
 291 be set as a boundary condition into and/or out of the study area, but can also be simulated with
 292 basement erosion.

293 The subsidence data is explained in the following section. Published boreholes and seismic lines
 294 offshore in the Taiwan Strait and onshore (Lin and Watts, 2002; Lin et al., 2003; Yu and Chou, 2001),

295 together with constructed depth maps (Fig. 5) for five key stratigraphic horizons defined in an earlier
 296 study (Nagel et al., 2013) provide a solid first approximation database. Constraints on sediment fluxes
 297 are obtained from combining modern river loads, denudation data and sediment volumes and
 298 presented in sub-section 3.3.

299

300 3.2. Foreland basin subsidence

301 The most important basin-scale controls on accommodation include sea-level changes and flexural
 302 subsidence related to lithospheric thickening and tectonic loads. The West Taiwan basin formed by
 303 flexural bending of the Asian passive margin in front of westward migrating thrust loads of the
 304 growing accretionary wedge (Lin et al., 2003). In order to better constrain subsidence of the
 305 sedimentary basin, backstripping techniques (using Airy isostasy) were applied to 28 boreholes and 9
 306 stratigraphic sections (Nagel et al., 2013; Watts and Ryan, 1976).

307 Backstripping is used to stepwise decompact and unload a borehole or stratigraphic section. The
 308 influence of water depth and sedimentation on total subsidence are extracted in order to isolate the
 309 contribution of tectonic subsidence alone. The tectonically driven subsidence at any location in the
 310 basin is given in Allen and Allen (2009):

$$TS = Y \cdot \left(\frac{\rho_m - \rho_s}{\rho_m - \rho_w} \right) - \Delta sl \cdot \left(\frac{\rho_w}{\rho_m - \rho_w} \right) + (W_d - \Delta sl)$$

311 where W_d is the average water depth at which the sedimentary units were deposited, Y is the
 312 decompact sediment thickness, and ρ_m , ρ_w , and ρ_s are densities of mantle, water and sediment, and
 313 Δsl is the difference in sea-level height h between the present and the time at which the sediments
 314 were deposited:

$$\Delta sl = \left(\frac{\rho_m - \rho_w}{\rho_m} \right) \cdot (h_2 - h_1)$$

315 The water depth at the time of deposition for the backstripped strata was estimated using
 316 paleobathymetries from depositional models of Nagel et al. (2013). Note that since sediments in the
 317 western foreland basin were deposited on a shallow marine continental shelf, the influence of the
 318 water column (10s of metres) on the backstripped strata is small relative to the considered sediment
 319 thicknesses (100s of metres). For decompaction, sediment was assumed to be composed of two main
 320 grain size classes, sand and mud, which correspond to the modern siliciclastic river supply and is
 321 consistent with detailed lithologic analysis (Huh et al., 2011; Nagel et al., 2013). When the basin gets
 322 progressively filled with sediments, mechanical compaction introduces loss of water during sediment
 323 burial and affects depth-porosity curves for different lithologies. The trend between porosity and depth
 324 is usually approximated by:

$$\phi = \phi_0 \cdot e^{-cy}$$

325 This produces an asymptotically low porosity with increasing depth, where ϕ_0 describes surface
 326 porosity and c the coefficient of compaction (Table 2). The flexure of the basement was computed
 327 with an elastic thickness of 15 km, a Young's modulus of 100 GPa and a Poisson's ratio of 0.25,
 328 chosen according to published values for the Taiwan foreland basin (Lin and Watts, 2002).

329

Lithology	Surface porosity [ϕ_0]	Compaction coefficient [km^{-1}]	Density [kg/m^{-3}]
Shales	0.63	0.51	2720
Sandstones	0.49	0.27	2650
Mudstones	0.56	0.39	2680
Water			1030
Mantle			3330

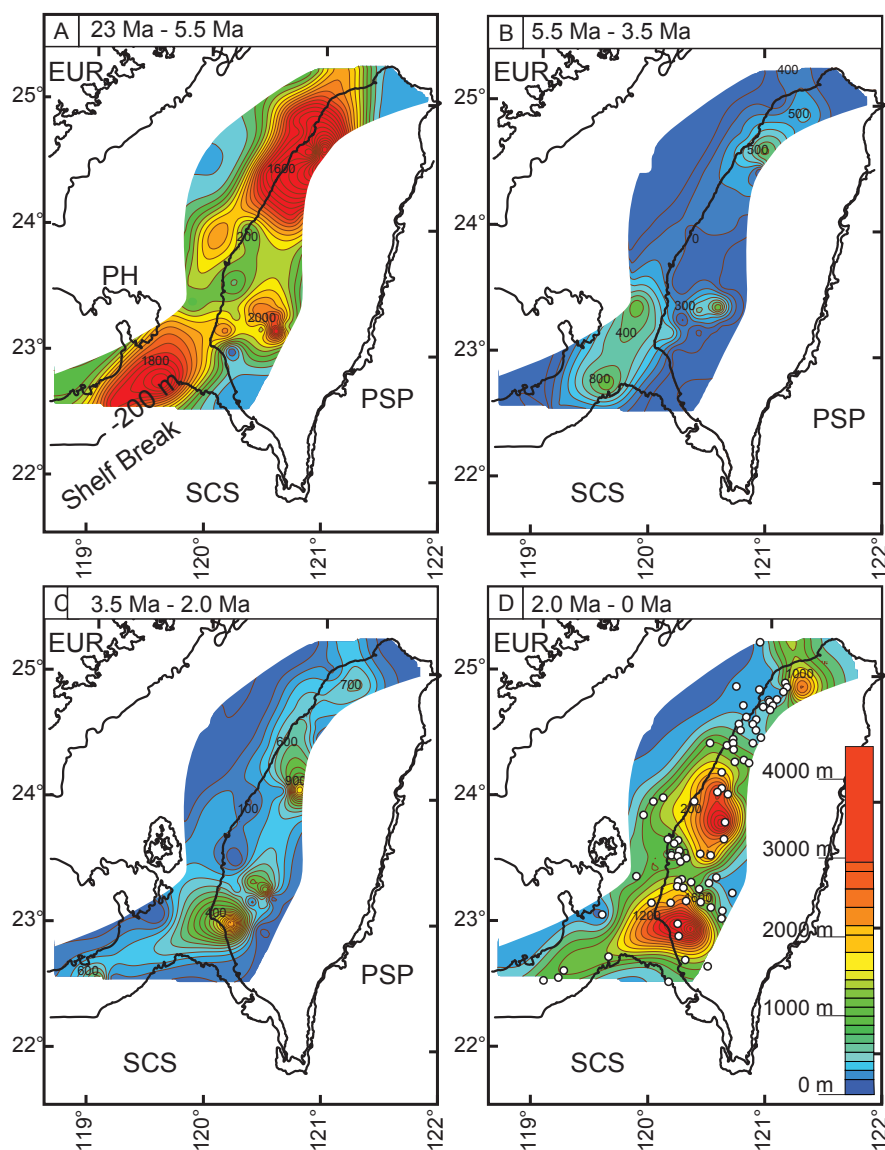
330

331 **Table 2:** Values used in the backstripping for the different lithologies observed in the Western Taiwan foreland basin and
 332 compaction coefficient (after Allen and Allen, 2009; Lin et al., 2003; Tensi et al., 2006).

333

334 Backstripping results provide a detailed record of the Asian passive margin subsidence and uplift
 335 history at the five key biostratigraphic horizons explained above (Fig. 5). Lin *et al* (2003) showed that
 336 the subsidence history of the Asian passive margin is strongly influenced by its syn- and post-rift
 337 history due to extension in the South China Sea (post-breakup extension from 30 to 21 Ma, thermal
 338 subsidence from 21 to 12.5 Ma and a second post-breakup extension from 12.5 to 6.5 Ma). Increased
 339 subsidence since the early Pliocene (Fig. 5D and Fig. 6) is ascribed to growth of the Taiwan orogen as
 340 it propagates westward, introducing deformation and increasing sedimentation rates in the basin
 341 (Chang and Chi, 1983; Mouthereau et al., 2001). In addition, Tensi et al. (2006) demonstrated that the
 342 load associated with initial foreland basin has migrated rapidly westward 1 Ma ago and was stabilized
 343 at the same time as the basin was buried under large quantities of sediments (alluvial and fluvial fans
 344 of the Toukoshan fm.).

345



346

347 **Figure 5:** Maps of decompacted sediment thickness in between the five key biostratigraphic (nannofossils) horizons of Nagel
 348 et al (2013). White dots in map of panel D represent location of Chinese Petroleum Company drill holes.

349

350 The reconstructed subsidence pattern (Fig. 6) is consistent with sediment isopach maps shown in
 351 Figure 5. The obtained subsidence history of each stratigraphic section can then be interpolated to the
 352 boundaries of the stratigraphic simulation project to produce subsidence maps (Fig. 7) that constitute a
 353 direct input into Dionisos. Subsidence pattern in between two key stratigraphic horizons is simply
 354 linearly interpreted between the two considered maps.

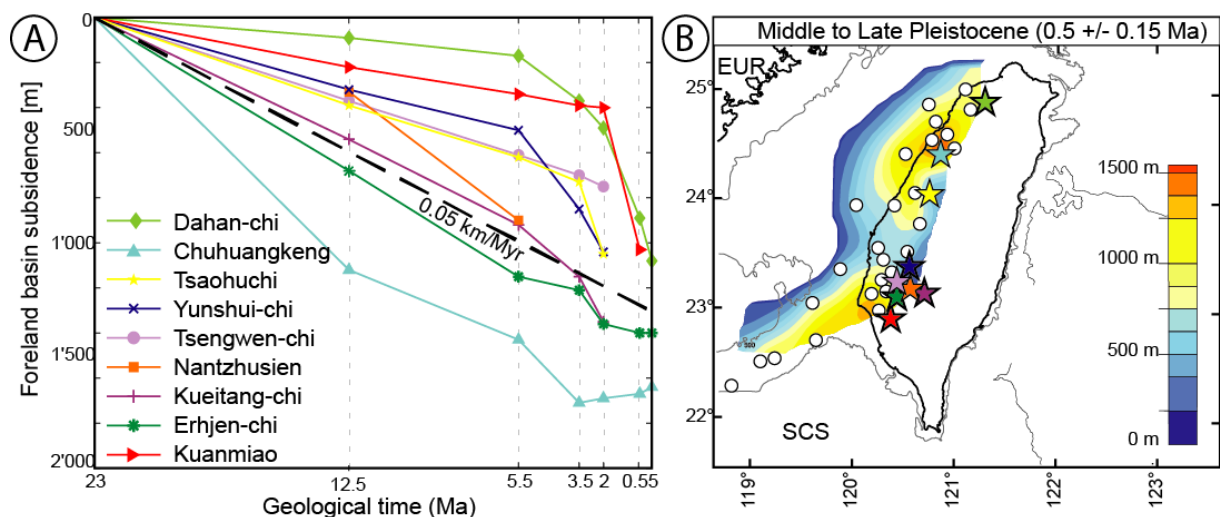
355 Lin and Watts (2002) showed that topography is insufficiently high to produce the observed
 356 subsidence pattern in an isostatic flexural model driven by surface loads. Following Simpson (2014), it
 357 can be proposed that this observation is an illustration of a possible decoupling between subsidence
 358 and surface loads, especially prominent in deeply eroded mountain ranges. In his model, Simpson
 359 explains that what may have been previously attributed to “buried loads” (as in Taiwan, e.g. Lin and
 360 Watts, 2002) could be related to accumulation through time of vertical deformation due to repeated
 361 large seismic events and dragging of the foreland margin by reverse slip on the main orogenic front.

362

363 3.3. Sediment fluxes and basin boundaries

364 The volume of sediment deposited in the basin was calculated from data of published boreholes drilled
 365 by the CPC (Chinese Petroleum Corporation) in the western foreland basin (Fig. 5) (e.g., Lin et al.,
 366 2003; Shaw, 1996). For each sequence the sediment thickness is extrapolated between the present day
 367 forebulge and the Western Foothills by a triangulation algorithm to obtain four maps between early
 368 Miocene and late Pleistocene (four maps in between the five key chronostratigraphic horizons, Fig. 5).

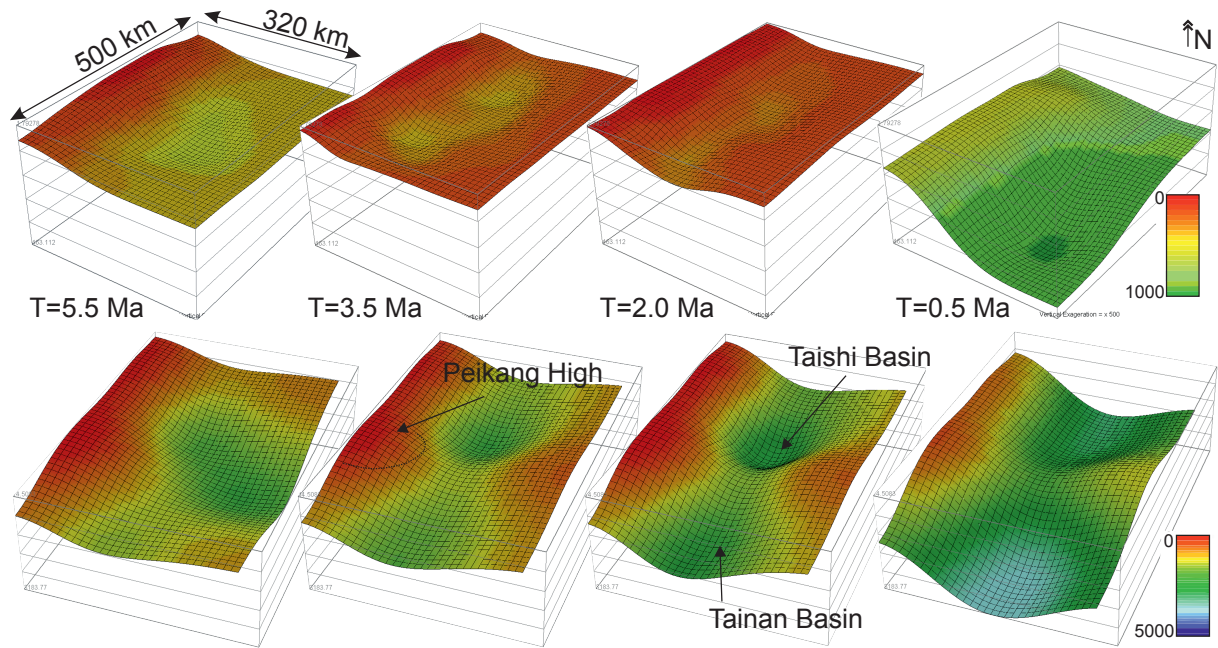
369



370

371 **Figure 6:** A) Tectonic subsidence histories from stratigraphic sections (each colored line correspond to a section) in the fold-
 372 and-thrust belt of Taiwan (marked with a star, ordered from north to south). The vertical dashed lines correspond to the five
 373 key chronostratigraphic horizons (see text) chosen to subdivide the foreland basin evolution in 4 stages. Dahan-chi (Pan,
 374 2011), Chuhuangkeng (Huang, 1976), Yunshuichi/Tsaohuchi (Yeh and Chang, 1991; Yeh and Yang, 1994), Tsengwen-chi
 375 (Chen et al., 2001a), Nantzhusien (Ting et al., 1991; Yu et al., 2008), Kueitangchi (Huang, 1977), Erhjen-chi (Hornig and
 376 Shea, 1994), Kuanmiao (Chiu, 1975). B) Tectonic subsidence map for the late Pleistocene (NN19/20) with 28 boreholes and
 377 9 stratigraphic sections. Stars indicate stratigraphic sections with color coding corresponding with left panel in which sections
 378 legend is ordered from North (top) to South (bottom).

379



380
 381 **Figure 7:** Smoothed subsidence maps for each simulated interval with tectonic subsidence used in the program (upper row)
 382 and total subsidence (including isostatic effects of sediment and water loading, lower row). The sediment depocenters in the
 383 north (e.g. Taishi basin) and the south (e.g. Tainan basin) are separated by the Peikang High.

384
 385

386 The sediment volume accumulated within each time sequence is shown in Table 3. A total of 82'000 to
 387 125'000 km³ of sediment accumulated since 5.5 Ma in the foreland basin of Taiwan. If we assume that

Age [Ma]	Sediment Volume [km ³]	Sediment Flux [km ³ /Ma]	Sediment Flux [km ³ /Ma] From Asia	Sediment Flux [km ³ /Ma] From Taiwan
0.0 - 2.0	47'214 - 64'884	23'607 - 32'442	..	17'864 - 28'203
2.0 - 3.5	20'443 - 35'980	13'628 - 23'987	..	7'885 - 19'748
<i>Total</i>	<i>67'657 - 100'864</i>			
3.5 - 5.5	15'917 - 26'502	7'959 - 13'251	..	6'594 - 9'012
5.5 - 23.5	76'298 - 103'383	4'239 - 5'743	4'239 - 5'743	0
<i>Total</i>	<i>159'872 - 230'749</i>			

388 collision started between 5.5 Ma and 3.5 Ma, and that before 5.5 Ma accumulated sediment thickness
 389 corresponded primarily to influx of material from Asia mainland, we interpret the increasing sediment
 390 influx from the Taiwan orogenic wedge to be in a range of 6'500 to 28'000 km³/Ma (Table 3). This
 391 sediment flux is probably overestimated since the basin also must have received material from its
 392 western border, i.e. Asia mainland. However, this contribution was probably swamped by the dramatic
 393 increase in sedimentation rates that accompanied Taiwan orogeny (Chang and Chi, 1983). In addition,
 394 some of the sediment transported into the foredeep consists of recycled foreland basin deposits.
 395 Therefore, calculated sedimentation rates over the area of modern foreland basin are lower when
 396 compared with sedimentation rates from Western Foothills, especially during the last phase of
 397 orogenesis from 2 Ma to 0 Ma (Chang and Chi, 1983).

398

399 **Table 3:** Sediment volume accumulated during the Neogene on the Asian passive margin calculated for the area between the
 400 modern forebulge and the Western Foothills (ca. 35'000 km²). The age sub-division corresponds to biostratigraphic key
 401 horizons from nannofossil zonation (Nagel et al., 2013). The first two digits are considered significant.

402

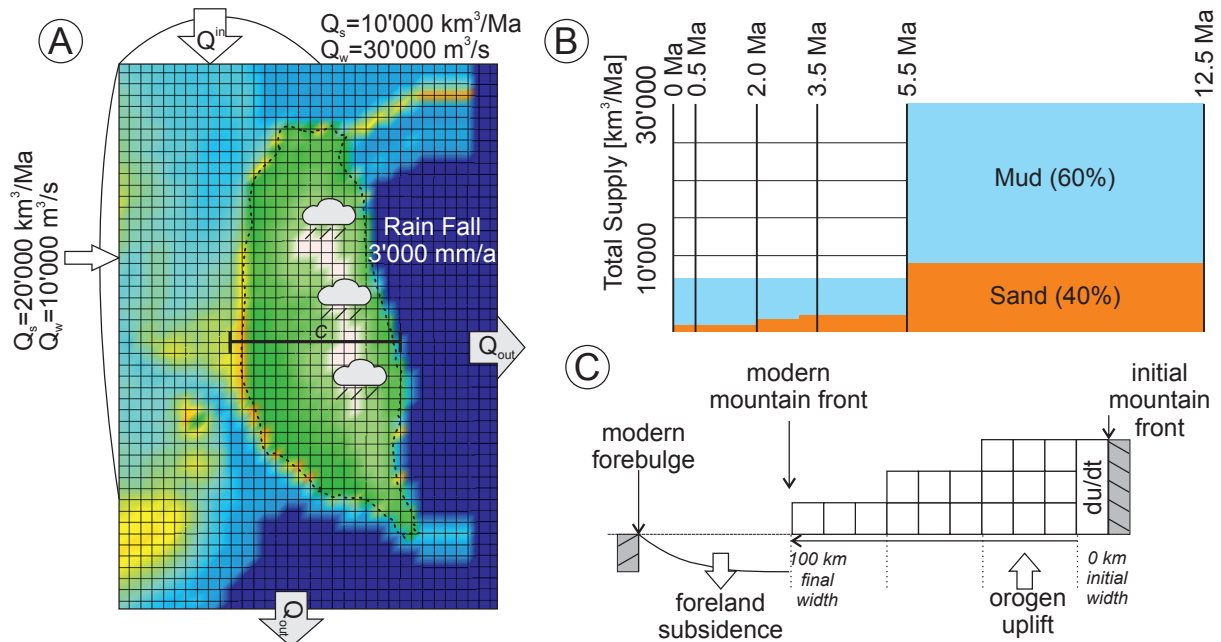
403 **Table 4:** Sediment volume accumulated in the Cenozoic sedimentary basins of Southeast Asia (modified from, Métivier et
 404 al., 1999).

405

406 In addition to previous consideration, sediment fluxes from the growing Taiwan orogen are
 407 constrained by comparing the amount of sediment that has been preserved in Taiwan foreland basin

Sediment Volumes SE Asia [km ³]		2 - 0 Ma	2 - 5 Ma	5 - 11 Ma	11 - 17 Ma	17 - 24 Ma	24 - 5 Ma	[km ³ /Ma]
Pearl River & S. Taiwan	Total	81000	93000	240000	85000	130000	455000	23947
	uncertainty	40000	38000	100000	31000	49000		
	min	61000	74000	190000	69500	105500	365000	19211
	max	101000	112000	290000	100500	154500	545000	28684
E. China Sea & N. Taiwan	Total	190000	200000	45000	39000	88000	172000	9053
	uncertainty	81000	75000	16000	12000	31000		
	min	149500	162500	37000	33000	72500	142500	7500
	max	230500	237500	53000	45000	103500	201500	10605
Okinawa Trough	Total	130000	99000	16000	5200	4900	26100	1374
	uncertainty	64000	40000	6000	2000	2100		
	min	98000	79000	13000	4200	3850	21050	1108
	max	162000	119000	19000	6200	5950	31150	1639
Total	Total	271000	293000	285000	124000	218000	653100	34374
	Min	210500	236500	227000	102500	178000	528550	27818
	Max	331500	349500	343000	145500	258000	777650	40929

408 with the amount of sediment accumulated in Cenozoic sedimentary basins north and south of Taiwan
 409 (Table 4). The obtained boundary supply fluxes are minimum, because some unknown amount might
 410 have bypassed or not even reached the Taiwan Strait.



411

412 **Figure 8:** Initial sediment supply history applied in the model. A) The two source areas correspond to Asia mainland (West)
 413 and the East China Sea (North). Rainfall follows the modern mean annual rainfall rate. The fluvial water discharge was
 414 estimated by modern river discharges in Southeast Asia (Table 5). B) The initial total sediment supply from the boundaries
 415 through time is based on the sediment preserved in the foreland basin and the sediment accumulation rates in Southeast Asia
 416 (Métivier et al., 1999). The grain size distribution follows modern suspended sediment concentrations and sea surface

417 measurements in the Taiwan Strait (Huh et al., 2011; Kao and Milliman, 2008; Xu et al., 2009), as well as observations in the
 418 ancient sedimentary record (Nagel et al., 2013). See text for discussion. C) Sketch of orogen growth as implemented in
 419 Dionisos: the area of uplift rate is progressively enlarged to simulate mountain range widening, from 0 at the onset to 100 km
 420 width at the end.

421
 422 Finally, initial sediment supply history imposed in the model is shown in Figure 8. Two sources of
 423 sediment are defined along the western and northern sides of the model box (Fig. 2). It is important to
 424 note that these sources refer to general provenances located along the model boundaries and are not
 425 meant to represent individual rivers. Today, only smaller tributaries of the Minjiang and Jiulong rivers
 426 drain directly into the Taiwan Strait, collectively discharging only 1/10 of Taiwanese rivers (Table 5).
 427 Water discharge per source area was assumed to be similar to modern water discharge of rivers in
 428 Southeast Asia (Table 5).

	catchment area [km^2]	mean channel gradient [m/km]	average water dis- charge [m^3/s]	dis- sediment load [km^3/a]	shelf gradient [m/km]
WORLD*					
Mississippi	2900000	0.5	17704	0.1481	8.0
Amazon	5700000	0.8	150000	0.4444	0.7
Ebro	85000	1.3	500	0.0074	3
Nile	4000000	1.6	2700	0.0889	4
Bengal	1750000	1.7	29700	0.3630	1.1
Indus	1400000	2.5	2644	0.1667	1.5
Sepik River	77700	0.05	3700	0.0288	6.50
Fly River	76000	-	6000	0.0315	0.76
Waiapu River	1734	-	1346	0.0181	5.00
SOUTHEAST ASIA**					
Yangtze	1940000	0.04	28507	0.1778	0.17
Red	124400	2	1200	0.0370	0.39
Pearl	440000	-	10654	0.0167	0.52
Yellow	750000	8.2	1160	0.4000	0.15
Minjiang	61000		6000	0.0028	
Jiulong	14700		1000	0.0009	
TAIWAN***					
Touchien	566	0.35	25	0.0078	2.3
Houlung	536	0.44	22	0.0181	1.8
Taan	758	0.34	36	0.0007	1.8
Tachia	1235	0.26	78	0.0011	1.4
Wu	2026	0.22	116	0.0019	0.8
Choshui	3155	0.18	120	0.0004	1.4
Peikang	645	0.06	27	0.0037	4.1
Pachang	475	0.24	23	0.0222	4.3
Tsengwen	1177	0.18	34	0.0007	4.3
Erjen	350	0.07	19	0.0007	5.0
Kaoping	3256	0.23	248	0.0059	5.0
Peinan	1603	0.44	97	0.0078	30.0
Hsiukuluan	1790	0.29	125	0.0130	50.0
Hualien	1507	0.4	100	0.0333	35.0
Hoping	556	0.37	37	0.0081	80.0
Lanyang	979	0.48	75	0.0111	13.0

*from Somme et al. 2009 and references therein, **Chen et al. 2001, Wang et al. 2005, Wang et al. 2007, Wang et al. 2008, Liu et al. 2007, Zhang et al. 2008, Olariu et al. 2009, Milliman and Syvitski 1992, Yu et al. 2006, Kineke et al. 2000, Huh et al. 2011, Kuehl et al. 2004, Kuehl et al. 2000, Yu et al. 1991, Wolanski et al. 1995, Kniskern et al. 2010, Hicks et al. 2000, ***Liu et al. 2008, Kao and Milliman 2008, Yu and Chiang 1997

429
 430 **Table 5:** Main parameters of rivers from Taiwan, Southeast Asia and larger rivers worldwide for comparison. Data World
 431 from Somme *et al* (2009) and references therein. Data for Southeast Asia from Chen *et al* (2001b), Hicks *et al* (2000), Huh *et*
 432 *al* (2011), Kineke *et al* (2000), Kniskern *et al* (2010), Kuehl *et al* (2004), Liu *et al* (2007), Milliman and Syvitski (1992),
 433 Olariu and Steel (2009), Wang *et al* (2007), Wang *et al* (2005), Wolanski *et al* (1995), Yu *et al* (1991), Yu and Huang (2006)
 434 and Zhang *et al* (2008). Data for Taiwan from Kao *et al* (2008), Kao and Milliman (2008), Liu *et al* (2008) and Yu *et al*
 435 (1997).

436
 437 Since sediment transport in Dionisos is modeled by diffusion, a short review of published values for
 438 the diffusivity coefficient K in different depositional environments is provided here for the sake of
 439 comparison with other studies having used a similar approach (Table 6). Although these studies did
 440 not all use diffusion in exactly the same way for modeling sediment transport (for instance depending
 441 on whether water discharge is taken into consideration or not), an average value for each depositional
 442 environment was used based on the values compiled in Table 6.

	Continental	Marine
Csato et al. (2007)	2000-4000	0.4-10
Clark et al. (2009)	1000-2000	0.01-1
Burgess et al. (2006)	125-500	2.5-10.0
Schlager and Adams (2001)	100	0.15
Flemings and Jordan (1989)	1-25.0	0.1-5
Jordan and Flemings (1991)	4-200	0.1-1
Sinclair et al. (1991)		0.5
Kaufman et al. (1991)		10.0-75
Rivenaes (1992)		0.05-10.0
Paola et al. (1992)	10.0-70.0	
Kenyon and Turcotte (1985)	24.0-560	
Naden et al. (1999)	191.0-3557	
Marr et al. (2000)	10-100	
Begin (1988)	4300	
Humphrey and Heller (1995)	0.25	

443

444

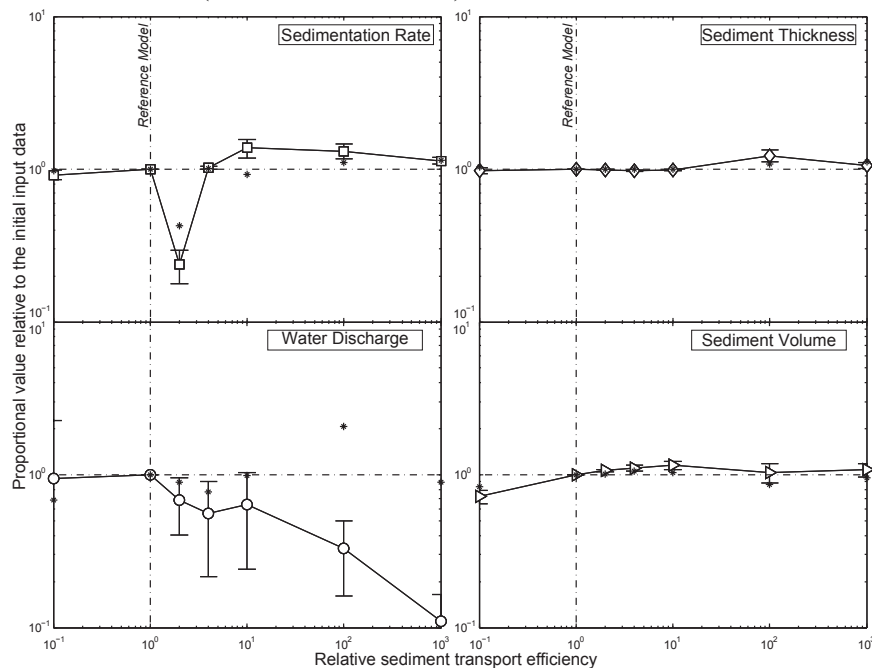
Table 6 Ranges of diffusion coefficients used in modeling studies for individual depositional environments. The values were converted to [km²/ka].

445

446

Figure 9 shows the sensitivity of different parameters (water discharge, sediment thickness, sediment volume, sedimentation rate) for 7 model runs with increasing sediment transport efficiencies (between 0.1xK_{initial} and 1000xK_{initial}, with K_{initial} being the diffusion coefficient of base model). All models were run with the standard model set-up described above. Parameters were measured at three different points within the basin at seismic lines #1, #2, and #5 (see Fig. 2) as well as the average value from 3.5 Ma to 0 Ma (marked with asterisk).

452



453

454

Figure 9: Sensitivity test for different diffusion coefficients. Proportional values of the four measured parameters in relation to the initial model input data within the foreland basin, plotted against the relative efficiency of sediment transport. The results are from seven separate model runs with the same initial reference model parameters, but different diffusion coefficients.

455

456

457

458

459

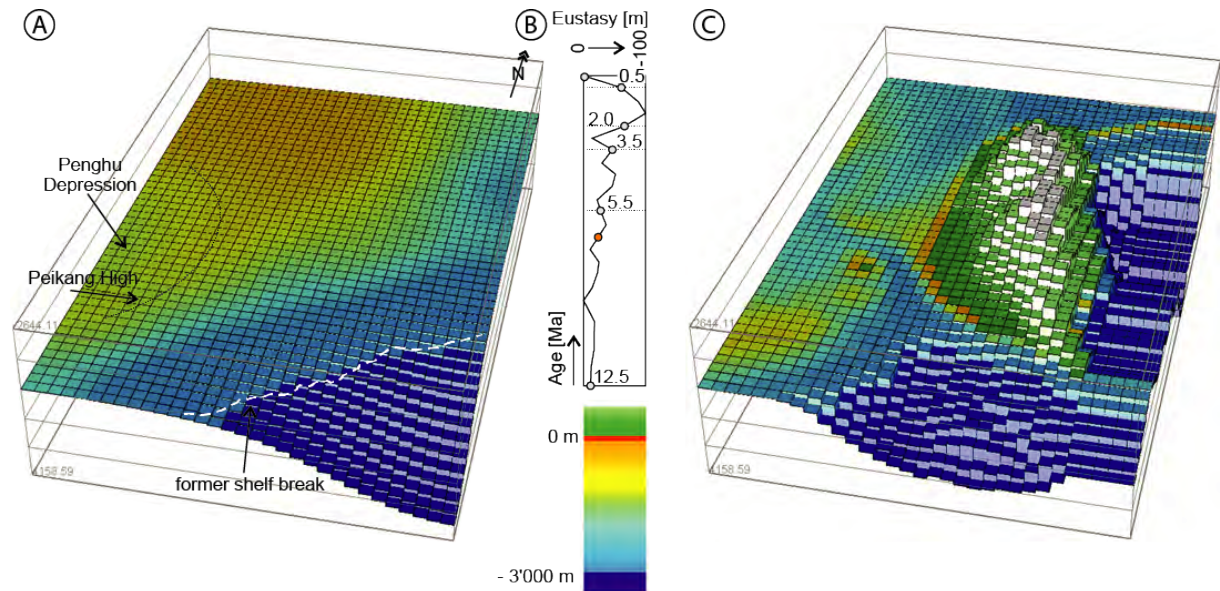
460

461

462

Simulations start at 12.5 Ma, which corresponds to the NN5-6 nannofossil boundary. This key biostratigraphic horizon has already been used in an earlier study to reconstruct the paleogeography during the arc-continent collision (Nagel et al., 2013). The study shows that sedimentation in the foreland basin during the Miocene to Pleistocene took place in a mixed storm- and tide-dominated

463 shallow marine depositional environment. Paleobathymetry did not change significantly from 12.5 Ma
 464 to 3.5 Ma (Fig. 10), when the basin started to subside due to the approaching orogenic wedge in the
 465 east and the mud-dominated Chinshui Shale was deposited (Fig. 3). It is important to note that
 466 progradation and shallowing-upward cycles associated with the approaching orogenic wedge took
 467 place earlier in the northern parts of the basin and progressed southward as the basin was filling up
 468 (Nagel et al., 2013).



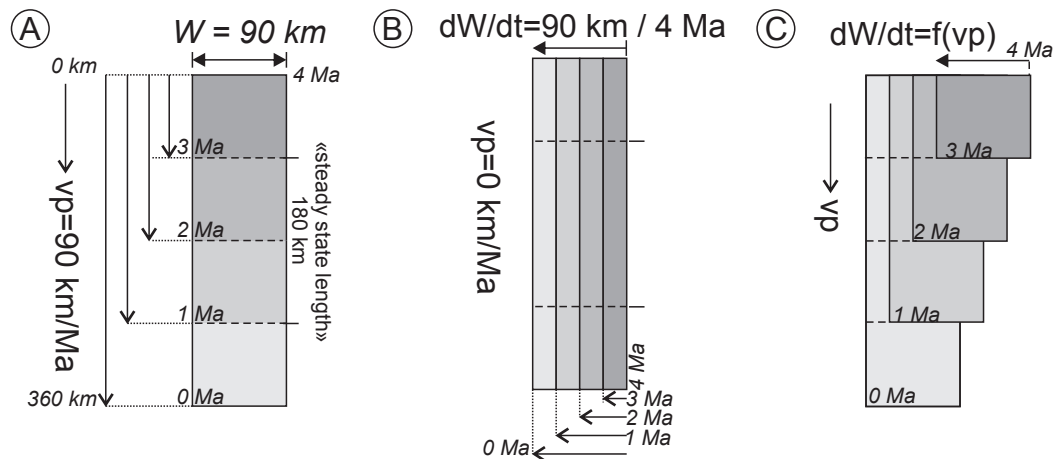
469

470 **Figure 10:** Initial bathymetry map at 12.5 Ma (A), and modern bathymetry (C). The 12.5 Ma map was constructed based on
 471 detailed facies analysis in the Western Foothills (Nagel et al., 2013). Sea level variation (B) after Miller et al. (2011) for
 472 indication.

473

474 3.4. Experimental setup

475 To explore the orogen growth history and basin architecture, three different tectonic scenarios were
 476 tested (Fig. 11). Each model considers the same initial boundary supply data (Fig. 8). In these
 477 experiments, orogenic uplift begins at ~ 4 Ma, which is in agreement with recent provenance studies
 478 (Nagel et al., 2013). The first orogenic growth model (Fig. 11A) considers southward propagation of
 479 the orogen at a rate of 90 km/Ma until present day length of 360 km is reached, and assumes a fixed
 480 steady state width of 90 km (Suppe, 1981). Using the time-space principle initially constructed by
 481 Suppe (1981), steady state size was reached after *ca* 1.3 Ma following onset of orogeny. In a second
 482 model (Fig. 11B) it is assumed that the orogen collided with a large promontory simultaneously along
 483 the length of the modern orogen, with no (or just minor) southward propagation. This scenario is based
 484 on sedimentological studies and paleogeographic reconstruction of Castellort et al (2011) and
 485 tectonic-thermochronometric data of Lee et al (2015). The third model, intermediate between both
 486 previous ones, (Fig. 11C) considers a linear growth in length of the orogen with time, along with
 487 lateral displacement of the orogen area as it overthrusts the Eurasian margin. In all three models, a
 488 continuous and constant uplift rate of 5 km/Ma was assumed. This rate covers the range of uplift rates
 489 that have been determined in Taiwan (Table 1).

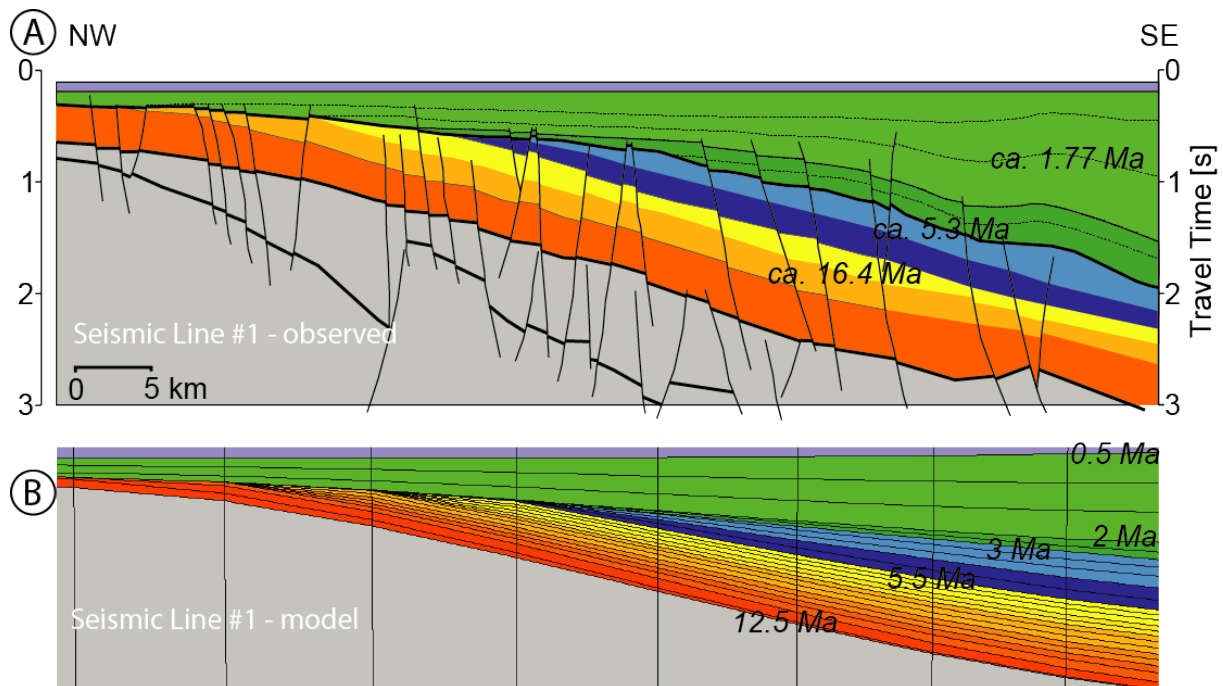


490
 491 **Figure 11:** Three orogen growth models tested in this study. A) Pure lengthening: southward propagation (90 km/Ma) of a
 492 steady state orogen with a fixed width of 90 km. B) Pure widening: lateral propagation, with a fixed length of 360 km. C)
 493 Lengthening and overthrusting: southwestward propagation of a steady state orogen.
 494

495 4. Simulation results and discussion

496 4.1. Foreland basin geometry

497 An initial test was performed to explore the adequacy of the imposed basin subsidence to reproduce
 498 the first order geometry observed on seismic lines in the Taiwan Strait (Fig. 4). A key horizon to
 499 compare is the transition from passive margin sedimentation to foreland basin sedimentation with the
 500 flexural forebulge unconformity as described above (Lin et al., 2003). As shown in Figure 12, the
 501 imposed timing and subsidence results in stratigraphic patterns (Fig. 12B) that correlate well with
 502 geometries observed in seismics (Fig. 12A).
 503



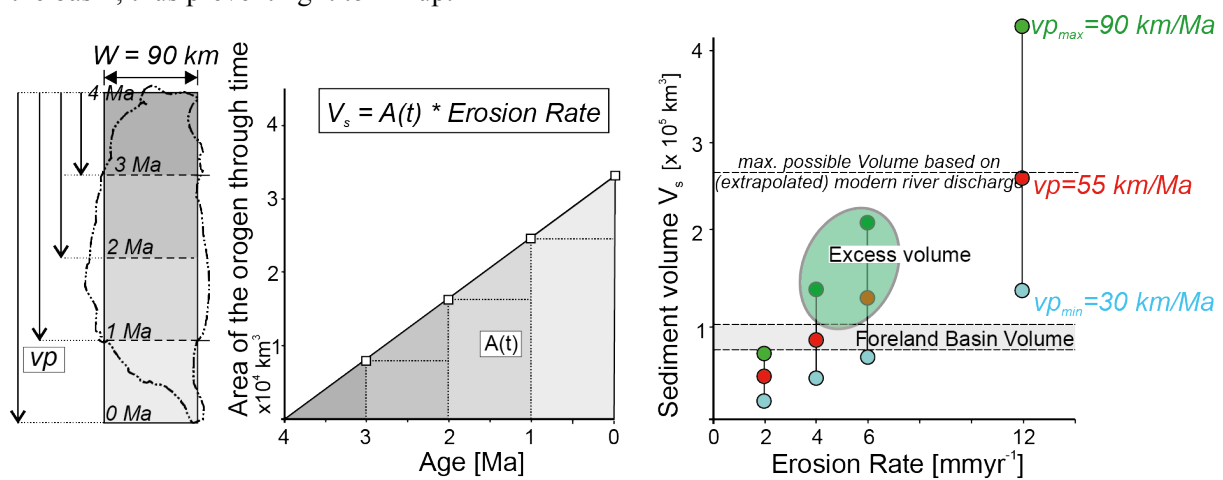
504
 505 **Figure 12:** A) Yu and Chou interpreted seismic line #1 (see location on Fig. 2). B) Cross-section at the position of
 506 seismic line #1 through simulated stratigraphy with Dionisos (this study). The input subsidence forces a dramatic change
 507 of sedimentation pattern at the transition from passive margin sedimentation to foreland sedimentation. This mimics the
 508 "flexural forebulge unconformity" documented by Yu and Chou (2001). This unconformity represents the boundary between

509 the pre-collisional Nanchuang Fm. and the syn-collisional Kueichulin Fm. and was estimated approximately at 6.5 Ma (Lin et
 510 al., 2003).

511

512 4.1. Mass flux calculations

513 Theoretical models of mountain building have proposed that an orogen can reach a topographic steady
 514 state when rates of rock uplift and erosion are balanced (Willett and Brandon, 2002). These models
 515 predict that, once steady state is reached, sediment flux into the basin exceeds available
 516 accommodation space because no additional tectonic load is acting on subsidence, and therefore the
 517 basin becomes overfilled with time (Covey, 1986; Naylor and Sinclair, 2008). Despite observations
 518 suggesting that the subaerial part of Taiwan's orogen has been in steady state since the Late Pliocene
 519 (Suppe, 1981, 1984), or even increased in exhumation rate in the Pleistocene (Hsu et al., 2016), the
 520 Western Foreland basin is still not overfilled. This can be explained either by a large original
 521 accommodation space (inherited from previous history) or by continuous removal of sediment from
 522 the basin, thus preventing it to fill-up.



523

524 **Figure 13:** A) Orogen growth model with a steady state orogen width of 90 km and a southward propagation rate of $V_p=30$
 525 to 90 km/Ma. B) The theoretical volume eroded from the mountain was calculated by integrating the orogen area through
 526 time multiplied by the erosion rate. C) The modern river discharge was extrapolated over 3.5 Ma and taken as an upper limit
 527 for the maximum possible sediment influx into the basin system (Table 5). The theoretical sediment volume eroded from the
 528 mountains and feeding the Western Foreland Basin was corrected for the fluvial discharge flowing to the east, which is
 529 currently 45% (Dadson et al., 2003).

530

531 To explore sediment dynamics within the foreland basin, mass balance calculations were done for a
 532 southward propagating orogen model. The total amount of material transported into the basin
 533 (according to tectonic scenario of Fig. 13) is compared with the amount of sediment preserved. The
 534 theoretical total amount of material, which has been eroded from the orogen since 4 Ma, is estimated
 535 by multiplying the integrated area (Fig. 13) with erosion rate (Table 1). Currently 55% of the annual
 536 fluvial sediment discharge is flowing West and 45% is drained East (Dadson et al., 2003; Liu et al.,
 537 2008). Hence the total sediment volume produced by the orogen was corrected for fluvial discharge
 538 flowing East.

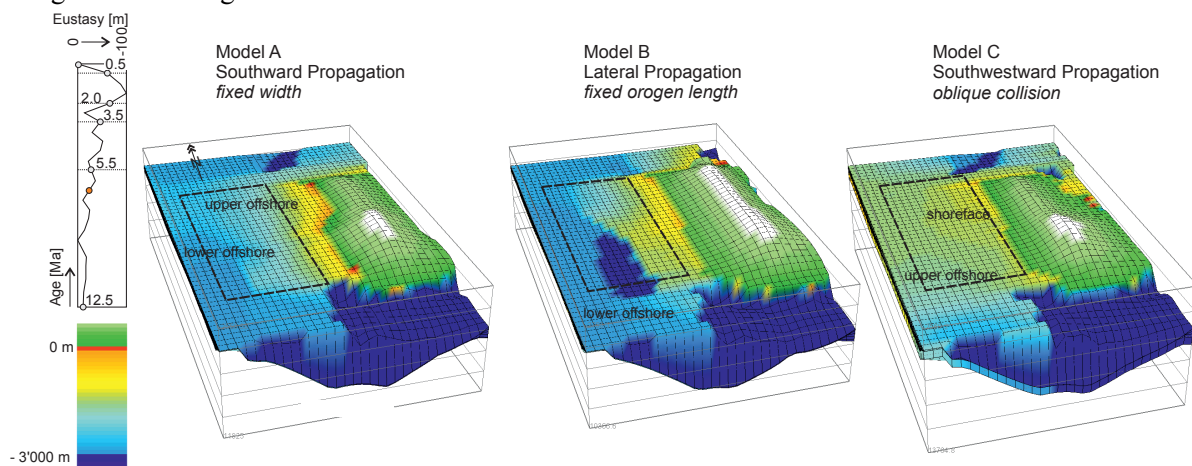
539 Figure 13 shows the potential sediment flux into the foredeep coming from the Taiwan mountains as
 540 estimated by the model. Computed fluxes vary from $25'000 \text{ km}^3$ (for a southward propagation rate of
 541 30 km/Ma and an average erosion rate of 2 mm/yr) and up to $425'000 \text{ km}^3$ (for a southward
 542 propagation rate of 90 km/Ma and an average erosion rate of 12 mm/yr), although this may be
 543 overestimated since it does not take into account the recycling of foredeep sediments. The current river
 544 sediment flux during typhoon season (Liu et al., 2008) was taken as an upper boundary for the
 545 maximum possible sediment influx, when extrapolated over 4 Ma (i.e., $285'000 \text{ km}^3$).

546 The amount of sediment preserved in the basin is much smaller than the possible amount of sediment
 547 brought into the basin (Fig. 13) when one considers a southward propagation rate of 90 km/Ma and
 548 erosion rates in a range of 4 to 6 km/Ma (Table 1). Our calculations suggest that between 25'000 km³
 549 and 115'000 km³ of material may have bypassed the foreland basin. If this is correct, it suggests that at
 550 least half the sediment eroded from the orogen may not be preserved in eventual foreland basin
 551 stratigraphic records. This material is likely longitudinally transported South, out of the basin (Nagel
 552 et al., 2013), and into the South China Sea. Observations in south-central Taiwan already indicate
 553 enhanced southward sediment transport since Late Pliocene marked by increasing amounts of
 554 submarine incisions (Fuh et al., 2003; Fuh et al., 1997). The southward sediment transport is also
 555 observed in the migration of sediment depocenters and facies belts, mainly driven by large sediment
 556 flux from the orogen (Nagel et al., 2013; Simoes et al., 2007).

557

558 4.2. Simulated sediment fluxes

559 An orogen that produces a steady flux of sediments was modeled for each of the three different growth
 560 scenarios in Figure 10 and the volume of material deposited in the basin was calculated for each
 561 scenario (Fig. 14). Steady state is established when the elevation of the mountain's top reaches a
 562 roughly constant value in less than 1 Ma. This is achieved by tuning the diffusion coefficient for
 563 continental sediment transport K , whereby an increase in K equals an increase in erosion, until a value
 564 of K is found that gives satisfactory results (mountain range elevation) for all 3 scenarios. Three
 565 different models were run, with a mean uplift rate set to 3, 5 and 12 mm/yr. Material is allowed to
 566 leave the basin to the south by diffusion. The area of the orogen at each time step is the same for each
 567 growth model, thus with identical uplift and erosion parameters the available material at each interval
 568 is assumed to be equal. This allows to compare the three models only in terms of their different
 569 tectonic growth scenario, and in terms of their implications for sediment transport in the basin
 570 alongstrike the orogen.



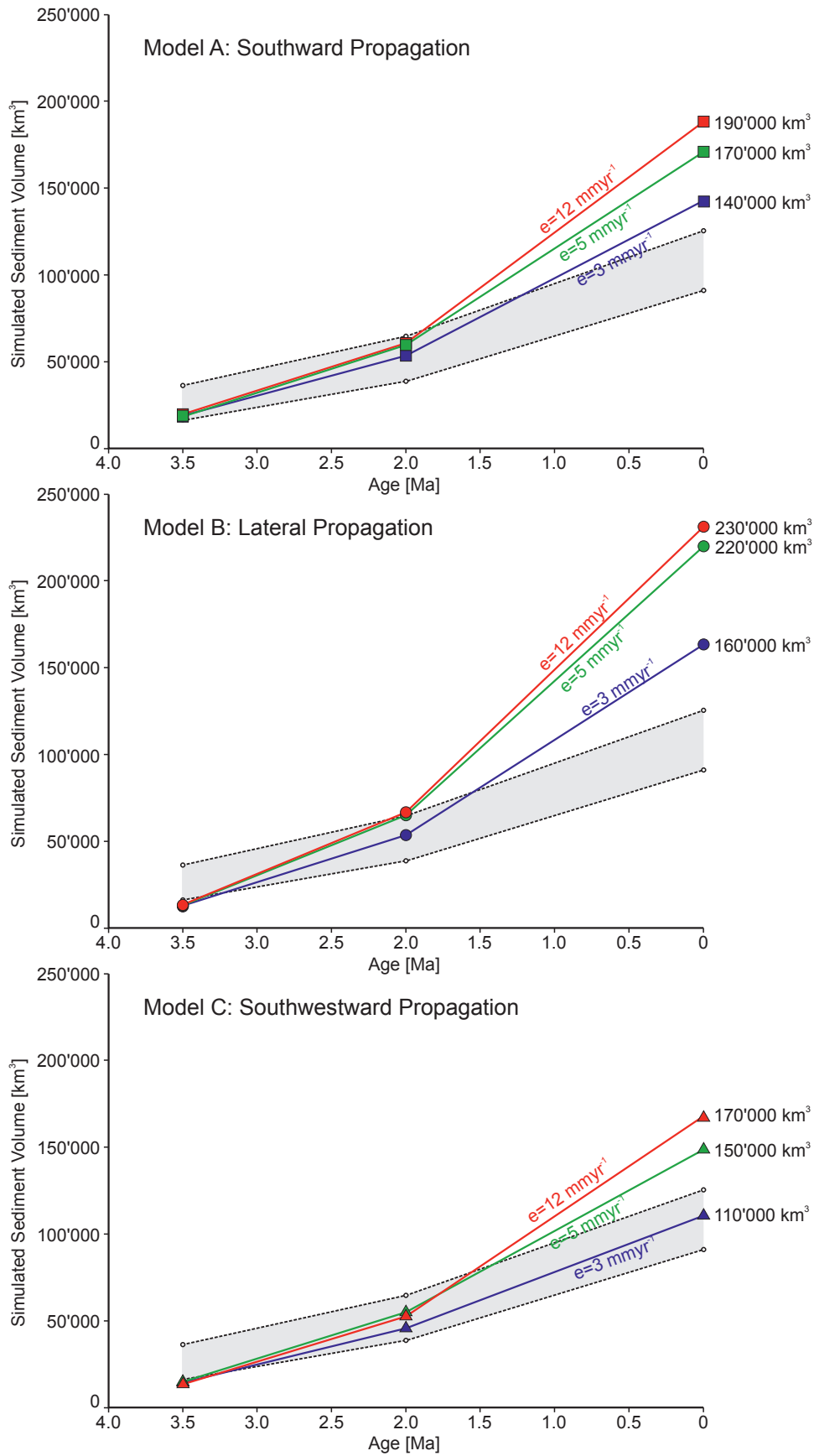
571

572 **Figure 14:** The model setup is shown schematically in Fig. 10. Model A is simulated with a southward propagation rate of 90
 573 km/Ma and a fixed width. In model B the length of the orogen was fixed and only lateral propagation allowed. Model C is a
 574 combined " oblique" collision, or southwestward propagation. In all the three models, the final orogen area and final
 575 erosional fluxes vary only by minor amount due to different erosional landscape evolution during relief growth. The area
 576 where the simulated foreland basin volume was measured is indicated with a black box.

577

578 The sediment volume of the foreland basin produced by each of the three models is shown in Figure
 579 15. The three standard models (southward, lateral, or oblique propagation) tend to overestimate the
 580 preserved sediment volume. Southward and oblique propagation achieve a better fit to observed
 581 sediment thicknesses than lateral propagation. Moreover lateral propagation did not accurately

582 reproduce foreland basin geometries. The best fit (geometry and volume) is achieved with the oblique
 583 collision scenario.



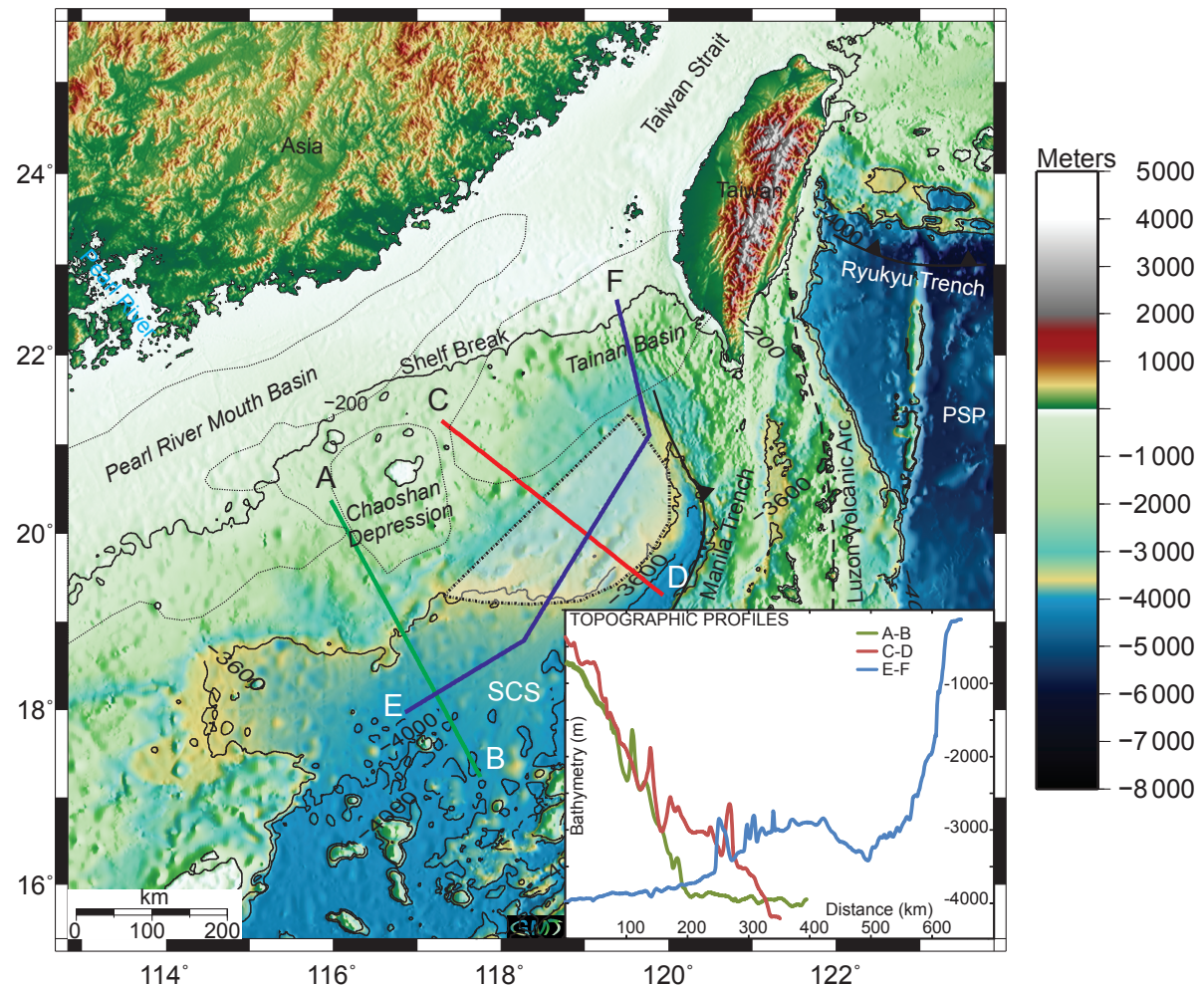
585 **Figure 15:** Calculated sediment volume in the foreland basin produced with the three standard collision models (Fig. 10).
586 The preserved sediment thickness in the Taiwan foreland basin is between 70-125'000 km³ (shaded area, see also Table 3).

587

588 The southward propagation models suggest an excess of sediment carried into the basin of between
589 15'000 and 80'000 km³. This amount is in agreement with the theoretical mass balance calculations
590 (Fig. 13). As observed, even though the orogen reached a steady state size as suggested by Suppe
591 (1981), due to longitudinal transport, the basin never becomes overfilled.

592 Earlier observations already implied an important longitudinal sediment transport out of the basin and
593 observations from the southwest of Taiwan seem to confirm these predictions (Covey, 1984; Yu and
594 Hong, 2006). Longitudinal sediment transport is common in most foreland basins. A good example is
595 the southern Pyrenees, where longitudinal sediment routing systems dominated a wedge-top depozone,
596 with deep marine sedimentation prevailing (Mutti, 1977, Castelltort et al., 2017). It is important to
597 note in contrast, that an averaged orogen-wide erosion rate of 3 mm/yr produces a sediment volume
598 that is consistent with the preserved sediment volume in the western foreland basin (Fig 15, Model C).
599 This means that, according to our approach, either previous estimates of erosion rate based on
600 thermochronological constraints are too high, or sediment bypass occurred at least for parts of basin
601 history.

602 Because of the presence of many submarine canyons draining sediment from the Taiwan Strait to the
603 deeper basin in the Manila trench (Damuth, 1979; Yu and Chang, 2002; Yu et al., 2009), a
604 fundamental unknown is whether one can find there the missing sediment volume suggested by our
605 calculations. Sparse literature data are available on the nature of the sedimentary basins in the area of
606 the South China Sea close to Taiwan (Lee et al., 1993; Lin et al., 2008; Yu and Huang, 2009), with a
607 main focus on the Pearl River delta and associated submarine fan deposits (Lüdmann et al., 2001; Su
608 et al., 1989; Xiong et al., 2004) (Li et al., 2008). A topographic map of the submarine regions south of
609 Taiwan indicates a peculiarity in the slope of the South China Sea continental margin compared to its
610 continuation further to the South. This suggests an anomalous accumulation of sediment in this area.
611 Topographic profiles across and along the continental margin (Fig. 16, inset) show that the ocean floor
612 remains at a bathymetry of about -4000 m. As a first order approximation we use the isobath -3600 m
613 and a line roughly parallel to the shelf edge to delimit the contour of this promontory of the continental
614 margin and to compute its volume. The volume enclosed by the area drawn on Figure 16 and using -
615 4000 m as a base elevation represents 28'700 km³ (15'400 km³ when -3600 m is used as a base
616 elevation for the calculation).



617
 618 **Figure 16: Digital elevation model of the South China Sea with topographic profiles across the submarine promontory**
 619 **of the -3'600m isobath. The volume stored in the shaded area (contoured with dashed line) represents $\sim 30'000 \text{ km}^3$.**
 620

621 The volume of this submarine topography is compatible with deposits originated in the Taiwan
 622 orogeny that would have bypassed the Taiwan Strait. The outline of Tainan basin on the topographic
 623 map of figure 16 and its southwestward orientation visible on paleogeographic maps of figure 5 show
 624 that Tainan basin may have constituted a longitudinal through working as a conduit for material
 625 sourced in Taiwan orogenic wedge. In this case, a non-negligible portion of the sedimentary record of
 626 mountain building may have been preserved outside of the foreland basin itself. However this
 627 hypothesis remains to be tested with future work investigating the sedimentological nature and
 628 stratigraphy of this anomalous promontory and look for potential sediment depocenters outside of the
 629 Taiwan Strait. This finding outlines the potential complexity of interpreting provenance signals
 630 (Romans et al., 2016) in orogen-basin systems with highly dynamic topographic evolution.

631

632 5. Conclusions

633 The sedimentary system of the Taiwan foreland basin is governed by oblique collision between Luzon
 634 volcanic arc and the Asian passive margin. Different geometrical models of orogen growth and its
 635 influence on basin architecture were tested by means of a stratigraphic modeling approach. By looking
 636 at sediment volumes in the foreland basin and calculating mass flux sediment budgets, we document
 637 that a significant (perhaps more than 50%) portion of the sediment eroded from the orogen is not

638 preserved in the stratigraphic record of the immediately adjacent foreland basin. The excess sediment
639 is most likely transported northwards into the Okinawa Trough and southwards into the South China
640 Sea, where large submarine channel-lobe systems developed. This interpretation is consistent with an
641 increasing amount of submarine incisions since Late Pliocene observed in southwest Taiwan.
642 We propose that this may explain why, despite being in front of a steady state orogen, the basin
643 remains in an "underfilled" state. We tested three different orogenic growth scenarios with
644 longitudinal transport. While predicted preserved sediment thicknesses exceeded observed sediment
645 thickness, longitudinal transport was efficient enough to keep the basin from overflowing in all three
646 scenarios. However, we find that, despite recent suggestions that collision in Taiwan may have been
647 synchronous along its entire length (over the length of Taiwan, Castelltort et al., 2011, Lee et al.,
648 2015), an oblique collision fits better the observed basin architecture.

649

650 **Acknowledgements**

651 This work was funded by Swiss National Science Foundation grant #200020-131890 to SC. We are
652 grateful to Adam Bumby for editorial work and an anonymous reviewer who greatly improved the
653 manuscript.

654 **References**

- 655 Abbott, L.D., Silver, E.A., Thompson, P.R., Filewicz, M.V., Schneider, C., Abdoerrias, 1994. Stratigraphic
656 constraints on the development and timing of arc-continent collision in northern Papua New Guinea. *J.*
657 *Sediment. Res.* 64, 169-183.
- 658 Allen, P.A., Allen, J.R., 2009. *Basin Analysis: Principles and Applications*. John Wiley & Sons.
- 659 Allen, P.A., Armitage, J.J., Carter, A., Duller, R.A., Michael, N.A., Sinclair, H.D., Whitchurch, A.L., and
660 Whittaker, A.C., 2013. The Qsproblem: Sediment volumetric balance of proximal foreland basin systems.
661 *Sedimentology*, v. 60, no. 1, p. 102–130, doi: 10.1111/sed.12015.
- 662 Allen, P.A., Crampton, S.L., Sinclair, H.D., 1991. The inception and early evolution of the North Alpine
663 Foreland Basin, Switzerland. *Basin Res.* 3, 143-163.
- 664 Begin, Z.B., 1988. Application of a diffusion-erosion model to alluvial channels which degrade due to base-level
665 lowering: *Earth Surface Processes and Landforms*, v. 13, no. 6, p. 487–500, doi: 10.13031/2013.34743.
- 666 Burgess, P.M., Lammers, H., van Oosterhout, C., and Granjeon, D., 2006. Multivariate sequence stratigraphy:
667 Tackling complexity and uncertainty with stratigraphic forward modeling, multiple scenarios, and conditional
668 frequency maps: *AAPG Bulletin*, v. 90, no. 12, p. 1883–1901, doi: 10.1306/06260605081.
- 669 Castelltort, S., Whittaker, A., Vergés, J., 2015. Tectonics, sedimentation and surface processes: from the
670 erosional engine to basin deposition. *Earth Surf. Process. Landforms* 40, 1839–1846. doi:10.1002/esp.3769
- 671 Castelltort, S., Nagel, S., Mouthereau, F., Lin, A.T.-S., Wetzel, A., Kaus, B., D., W.S., Chiang, S.-P., Chiu, W.-
672 Y., 2011. Sedimentology of early Pliocene sandstones in the south-western Taiwan foreland: Implications for
673 basin physiography in the early stages of collision. *J. Asian Earth Sci.* 40, 52-71.
- 674 Castelltort, S., Honegger, L., Adatte, T., Clark, J.D., Puigdefabregas, C., Spangenberg, J.E., Dykstra, M.L.,
675 Fildani, A., 2017. Detecting eustatic and tectonic signals with carbon isotopes in deep-marine strata, Eocene
676 Ainsa Basin, Spanish Pyrenees. *Geology* G39068.1. doi:10.1130/G39068.1
- 677 Chang, S.S.L., Chi, W.-R., 1983. Neogene nannoplankton biostratigraphy in Taiwan and the tectonic
678 implications. *Petroleum Geology of Taiwan* 19, 93-147.
- 679 Chang S. L., J. Yuan, P. T. Hsiao, and W. R. Chi, 1983, The Neogene series, tectonic evolution and petroleum
680 potentialities of southwestern Taiwan, in *Transactions of the Third Circum-Pacific Energy and Mineral*
681 *Resources Conferences*, vol. 3, edited by T. Wilson-Stuart, pp. 577 – 587.
- 682 Chen, W.-S., Huang, M.T., Liu, T.-K., 1991. Neotectonic significance of the Chimei Fault in the Coastal Range,
683 Eastern Taiwan. *Proc. Geological Society of China* 34(1), 43-56.

- 684 Chen, W.-S., Ridgway, K.D., Horng, C.-S., Chen, Y.-G., Shea, K.-S., Yeh, M.-G., 2001a. Stratigraphic
685 architecture, magnetostratigraphy and incised-valley systems of the Pliocene-Pleistocene collisional marine
686 foreland basin Taiwan. *Geol. Soc. Am. Bull.* 113, 1249-1271.
- 687 Chen, Z., Li, J., Shen, H., Zhanghua, W., 2001b. Yangtze River of China: historical analysis of discharge
688 variability and sediment flux. *Geomorphology* 41, 77-91.
- 689 Chiang, C.-S., Yu, H.-S., Chou, Y.-W., 2004. Characteristics of the wedge-top depozone of the southern Taiwan
690 foreland basin system. *Basin Res.* 16, 65-78.
- 691 Ching, K.-E., Hsieh, M.-L., Johnson, K.M., Chen, K.-H., Rau, R.-J., Yang, M., 2011. Modern vertical
692 deformation rates and mountain building in Taiwan from precise leveling and continuous GPS observations,
693 2000-2008, *J. Geophys. Res.*, 116, B08406, doi:10.1029/2011JB008242.
- 694 Chiu, H.T., 1975. Miocene stratigraphy and its relation to the palaeogene rocks in west-central Taiwan.
695 *Petroleum Geology of Taiwan* 12, 51-80.
- 696 Chou, J.-T., 1973. Sedimentology and paleogeography of the upper Cenozoic system of Western Taiwan.
697 *Proceedings of the Geological Society of China* 16, 111-143.
- 698 Clark, S. R., Bruaset, A. M., Sømme, T. O. and Løseth, T. M., 2009. A Flexible Stochastic Approach to
699 Constraining Uncertainty in Forward Stratigraphic Models. 18th World IMACS / MODSIM Congress, Cairns,
700 Australia 13-17 July 2009 <http://mssanz.org.au/modsim09>
- 701 Covey, M., 1984. Sedimentary and tectonic evolution of the western Taiwan Foredeep. Unpublished Ph.D.
702 thesis.
- 703 Covey, M., 1986. The Evolution of Foreland Basins to Steady State: Evidence from the Western Taiwan
704 Foreland Basin, *Foreland Basins*. Blackwell Publishing Ltd., pp. 77-90.
- 705 Dadson, S., Hovius, N., Pegg, S., Dade, W.B., Horng, M.J., Chen, H., 2005. Hyperpycnal river flows from an
706 active mountain belt. *J. Geophys. Res.* 110, F04016.
- 707 Dadson, S.J., Hovius, N., Chen, H., Dade, W.B., Hsieh, M.L., Willett, S.D., Hu, J.C., Horng, M.J., Chen, M.C.,
708 Stark, C.P., Lague, D., Lin, J.C., 2003. Links between erosion, runoff variability and seismicity in the Taiwan
709 Orogen. *Nature (London)* 426, 648-651.
- 710 Damuth, J.E., 1979. Migrating sediment waves created by turbidity currents in the northern South China Basin.
711 *Geology* 7, 520-523.
- 712 Dorsey, R.J., Buchovecky, E.J., Lundberg, N., 1988. Clay mineralogy of Pliocene-Pleistocene mudstones,
713 eastern Taiwan: combined effects of burial diagenesis and provenance unroofing. *Geology* 16, 944-947.
- 714 Dorsey, R.J., Lundberg, N., 1988. Lithofacies analysis and basin reconstruction of the Plio-Pleistocene
715 collisional basin, Coastal Range of Eastern Taiwan. *Acta Geol. Taiwan.* 26, 57-132.
- 716 Flemings, P.B., Jordan, T.E., 1989. A Synthetic Stratigraphic Model of Foreland Basin Development. *J.*
717 *Geophys. Res.* 94, 3851-3866.
- 718 Fuh, S.-C., Liang, S.-C., Wu, M.-S., 2003. Spatial and temporal evolution of the Plio-Pleistocene submarine
719 canyons between Potzu and Tainan, Taiwan. *Petroleum Geology of Taiwan* 36, 1-18.
- 720 Fuh, S.-C., Liu, C.-S., Wu, M.-S., 1997. Migration of canyon systems from Pliocene to Pleistocene in area
721 between Hsuning structure and Kaoping slope and its application for hydrocarbon exploration. *Petroleum*
722 *Geology of Taiwan* 31.
- 723 Fuller, C., Willett, S.D., Hovius, N., Slingerland, R., 2003. Erosion Rates for Taiwan Mountain Basins: New
724 Determinations from Suspended Sediment Records and a Stochastic Model of Their Temporal Variation. *The*
725 *Journal of Geology* 111, 71-87.
- 726 Fuller, C.W., Willett, S.D., Fisher, D., Lu, C.Y., 2006. A thermomechanical wedge model of Taiwan constrained
727 by fission-track thermochronometry. *Tectonophysics* 425, 1-24.
- 728 Garzanti, E., Vezzoli, G., Andò, S., Paparella, P., Clift, P.D., 2005. Petrology of Indus River sands: a key to
729 interpret erosion history of the Western Himalayan Syntaxis. *Earth Planet. Sci. Lett.* 229, 287-302.
- 730 Garzanti, E., Vezzoli, G., Lombardo, B., Andò, S., Mauri, E., Monguzzi, S., Russo, M., 2004. Collision-orogen
731 provenance (Western Alps): detrital signatures and unroofing trends. *The Journal of Geology* 112, 145-164.
- 732 Granjeon, D., 1997. Modélisation stratigraphique déterministe: conception et applications d'un modèle diffusif
733 3D multilithologique, *Géosciences. Université de Rennes, Rennes*, 200 p.
- 734 Granjeon, D., Joseph, P., 1999. Concepts and applications of a 3-D multiple lithology, diffusive model in
735 stratigraphic modeling, in: Harbaugh, J.W., Watney, W.L., Rankey, E.C., Slingerland, R., Goldstein, R.H.,

- 736 Franseen, E.K. (Eds.), Numerical Experiments in Stratigraphy. SEPM (Society for Sedimentary Geology), pp.
737 197-210.
- 738 Hall, R., 1996. Reconstructing Cenozoic SE Asia. Geological Society, London, Special Publications 106, 153-
739 184.
- 740 Hicks, D.M., Gomez, B., Trustrum, N.A., 2000. Erosion thresholds and suspended sediment yields, Waipaoa
741 River Basin, New Zealand. *Water Resour. Res.* 36, 1129-1142.
- 742 Ho, C.S., 1988. An introduction to the geology of Taiwan: explanatory text of the geologic map of Taiwan, 2nd
743 ed. Central Geological Survey, The Ministry of Economic Affairs, R.O.C. Taiwan.
- 744 Horng, C.-S., Huh, C.-A., 2011. Magnetic properties as tracers for source-to-sink dispersal of sediments: A case
745 study in the Taiwan Strait. *Earth Planet. Sci. Lett.* 309, 141-152.
- 746 Horng, C.-S., Huh, C.-A., Chen, K.-H., Lin, C.-H., Shea, K.-S., Hsiung, K.-H., 2012. Pyrrhotite as a tracer for
747 denudation of the Taiwan orogen. *Geochem. Geophys. Geosyst.* 13, Q08Z47.
- 748 Horng, C.-S., Shea, K.-S., 1994. Study of nannofossil biostratigraphy in the Eastern part of the Erhjen-Chi
749 section, Southwestern Taiwan. Special Publication of the Central Geological Survey 8, 181-204.
- 750 Hsu, W.-H., Byrne, T.B., Ouimet, W., Lee, Y.-H., Chen, Y.-G., Soest, M.V., Hodges, K., 2016. Pleistocene
751 onset of rapid, punctuated exhumation in the eastern Central Range of the Taiwan orogenic belt. *geology* 44,
752 719–722. doi:10.1130/G37914.1
- 753 Hsieh, M.L., Knuepfer, P.L.K., 2002. Synchronicity and morphology of Holocene river terraces in the
754 Southwestern Foothills, Taiwan: A guide to interpreting and correlating erosional river terraces across growing
755 anticlines: in Byrne, T.B. and Liu, C.-S., eds., *Geology and Geophysics of an Arc-Continent Collision, Taiwan*.
756 GSA Special Paper 358, 55-74.
- 757 Hu, J., Kawamura, H., Li, C., Hong, H., Jiang, Y., 2010. Review on current and seawater volume transport
758 through the Taiwan Strait. *J. Oceanogr.* 66, 591-610.
- 759 Huang, C.-Y., Yuan, P.B., Tsao, S.-J., 2006. Temporal and spatial records of active arc-continent collision in
760 Taiwan: A synthesis. *GSA Bulletin* 118, 274-288.
- 761 Huang, T.-C., 1976. Neogene calcareous nannoplankton biostratigraphy viewed from the Chuhuangkeng section,
762 Northwestern Taiwan. *Proceedings of the Geological Society of China* 19, 7-24.
- 763 Huang, T., 1977. Late neogene planktonic foraminiferal biostratigraphy of the Tainan Foothills region, Tainan,
764 Taiwan. *Petroleum Geology of Taiwan* 14, 121-145.
- 765 Huang, T., Huang, T.-C., 1984. Neogene biostratigraphy of Taiwan, in: Ikebe, N., Tsuchi, R. (Eds.), *Pacific*
766 *Neogen Datum Planes: contributions to biostratigraphy and chronology*. University of Tokyo Press.
- 767 Huh, C.-A., Chen, W., Hsu, F.-H., Su, C.-C., Chiu, J.-K., Lin, S., Liu, C.-S., Huang, B.-J., 2011. Modern (<100
768 years) sedimentation in the Taiwan Strait: Rates and source-to-sink pathways elucidated from radionuclides and
769 particle size distribution. *Cont. Shelf Res.* 31, 47-63.
- 770 Humphrey, N.F., and Heller, P.L., 1995. Natural oscillations in coupled geomorphic systems: An alternative
771 origin for cyclic sedimentation: *Geology*, v. 23, no. 6, p. 499–502.
- 772 Jahn, B.-M., Martineau, F., Peucat, J. J., Cornichet, J., 1986. Geochronology of the Tananao Schist Complex,
773 Taiwan, and its regional tectonic significance. *Tectonophysics* 125, 103-124.
- 774 Jan, S., Wang, J., Chern, C.-S., Chao, S.-Y., 2002. Seasonal variation of the circulation in the Taiwan Strait.
775 *Journal of Marine Systems* 35, 249-268.
- 776 Flemings, P.E., and Jordan, T.E., 1989. A Synthetic Stratigraphic Model of Foreland Basin Development. *J.*
777 *Geophys. Res.*, 94, p. 3851–3866.
- 778 Kaufman, P., Grotzinger, J. P., and McCormick, D. S., 1991. Depth-dependent diffusion algorithm for
779 simulation of sedimentation in shallow marine depositional systems. *Bulletin - Kansas Geological Survey*, 233 .
780 pp. 489-508. ISSN 0097-4471
- 781 Kao, H., Huang, G.-C., Liu, C.-S., 2000. Transition from oblique subduction to collision in the northern Luzon
782 arc-Taiwan region: Constraints from bathymetry and seismic observations. *J. Geophys. Res.* 105, 3059-3079.
- 783 Kao, S.-J., Jan, S., Hsu, S.-C., Lee, T.-Y., Dai, M., 2008. Sediment budget in the Taiwan Strait with high fluvial
784 sediment inputs from mountainous rivers: new observations and synthesis. *Terr. Atmos. Ocean Sci.* 19, 525-546.
- 785 Kao, S.J., Milliman, J.D., 2008. Water and Sediment Discharge from Small Mountainous Rivers, Taiwan: The
786 Roles of Lithology, Episodic Events, and Human Activities. *The Journal of Geology* 116, 431-448.

- 787 Kenyon, P.M., and Turcotte, D.L., 1985, Morphology of a delta prograding by bulk sediment transport:
788 Geological Society of America Bulletin, v. 96, no. 11, p. 1457, doi: 10.1130/0016-
789 7606(1985)96<1457:MOADPB>2.0.CO;2.
- 790 Kineke, G.C., Woolfe, K.J., Kuehl, S.A., Milliman, J.D., Dellapenna, T.M., Purdon, R.G., 2000. Sediment export
791 from the Sepik River, Papua New Guinea: evidence for a divergent sediment plume. *Cont. Shelf Res.* 20, 2239-
792 2266.
- 793 Kniskern, T.A., Kuehl, S.A., Harris, C.K., Carter, L., 2010. Sediment accumulation patterns and fine-scale strata
794 formation on the Waiapu River shelf, New Zealand. *Mar. Geol.* 270, 188-201.
- 795 Kuehl, S.A., Brunskill, G.J., Burns, K., Fugate, D., Kniskern, T., Meneghini, L., 2004. Nature of sediment
796 dispersal off the Sepik River, Papua New Guinea: preliminary sediment budget and implications for margin
797 processes. *Cont. Shelf Res.* 24, 2417-2429.
- 798 Lee, T.-Y., Lawver, L.A., 1995. Cenozoic plate reconstruction of Southeast Asia. *Tectonophysics* 251, 85-138.
- 799 Lee, T.-Y., Tang, C.H., Ting, J.-S., Hsu, Y.-Y., 1993. Sequence stratigraphy of the Tainan Basin, offshore
800 Southwestern Taiwan. *Petroleum Geology of Taiwan* 28, 119-158.
- 801 Lee, Y.-H., Chen, C.-C., Liu, T.-K., Ho, H.-C., Lu, H.-Y., Lo, W., 2006. Mountain building mechanisms in the
802 Southern Central Range of the Taiwan Orogenic Belt - From accretionary wedge deformation to arc-continental
803 collision. *Earth Planet. Sci. Lett.* 252, 413-422.
- 804 Lee, Y.H., Byrne, T., Wang, W.H., Lo, W., Rau, R.J., Lu, H.Y., 2015. Simultaneous mountain building in the
805 Taiwan orogenic belt. *geology* 43, 451-454. doi:10.1130/G36373.1
- 806 Li, C.-F., Zhou, Z., Hao, H., Chen, H., Wang, J., Chen, B., Wu, J., 2008. Late Mesozoic tectonic structure and
807 evolution along the present-day northeastern South China Sea continental margin. *J. Asian Earth Sci.* 31, 546-
808 561.
- 809 Liao, H.-R., Yu, H.-S., Su, C.-C., 2008. Morphology and sedimentation of sand bodies in the tidal shelf sea of
810 eastern Taiwan Strait. *Mar. Geol.* 248, 161-178.
- 811 Liew, P.-M., Pirazzoli, P.A., Hsieh, M.-L., Arnold, M., Barousseau, J.P., Fontugne, M., Giresse, P. 1993.
812 Holocene tectonic uplift deduced from elevated shorelines, eastern Coastal Range of Taiwan. *Tectonophysics*,
813 222(1), 55-68.
- 814 Lihou, J.C., Allen, P.A., 1996. Importance of inherited rift margin structures in the early North Alpine Foreland
815 Basin, Switzerland. *Basin Res.* 8, 425-442.
- 816 Lin, A.T., Liu, C.-S., Lin, C.-C., Schnurle, P., Chen, G.-Y., Liao, W.-Z., Teng, L.S., Chuang, H.-J., Wu, M.-S.,
817 2008. Tectonic features associated with the overriding of an accretionary wedge on top of a rifted continental
818 margin: An example from Taiwan. *Mar. Geol.* 255, 186-203.
- 819 Lin, A.T., Watts, A.B., 2002. Origin of the West Taiwan basin by orogenic loading and flexure of a rifted
820 continental margin. *J. Geophys. Res.* 107, 2185.
- 821 Lin, A.T., Watts, A.B., Hesselbo, S.P., 2003. Cenozoic stratigraphy and subsidence history of the South China
822 Sea margin in the Taiwan region. *Basin Res.* 15, 453-478.
- 823 Liu, C. H., 1995. Geodetic monitoring of mountain building in Taiwan, *EOS Trans. AGU*, 76, 636.
- 824 Liu, J.P., Liu, C.S., Xu, K.H., Milliman, J.D., Chiu, J.K., Kao, S.J., Lin, S.W., 2008. Flux and fate of small
825 mountainous rivers derived sediments into the Taiwan Strait. *Mar. Geol.* 256, 65-76.
- 826 Liu, J.P., Xu, K.H., Li, A.C., Milliman, J.D., Velozzi, D.M., Xiao, S.B., Yang, Z.S., 2007. Flux and fate of
827 Yangtze river sediment delivered to the East China Sea. *Geomorphology* 85, 208-224.
- 828 Liu, T.-K. 1982. Tectonic implication of fission track ages from the Central Range, Taiwan. *Proc. Geological*
829 *Society of China*, 25, 22-37.
- 830 Liu, T.-K., Chen, Y.-G., Chen, W.-S., Jiang, S.-H., 2000. Fission-track constraints on timing of peak
831 metamorphic temperature and rates of cooling and denudation of the early Central Range, Taiwan.
832 *Tectonophysics* 320, 69-82.
- 833 Liu, T.-K., Hsieh, S., Chen, Y.-G., Chen, W.-S., 2001. Thermo-kinematic evolution of the Taiwan oblique-
834 collision mountain belt as revealed by zircon fission track dating. *Earth Planet. Sci. Lett.* 186, 45-56.
- 835 Liu, T.K., Chen, Y.G., Chen, W.S., Jiang, S.H., 2000. Rates of cooling and denudation of the Early Penglai
836 Orogeny, Taiwan, as assessed by fission-track constraints. *Tectonophysics* 320, 69-82.
- 837 Liu, Z., Colin, C., Li, X., Zhao, Y., Tuo, S., Chen, Z., Siringan, F.P., Liu, J.T., Huang, C.-Y., You, C.-F., Huang,
838 K.-F., 2010. Clay mineral distribution in surface sediments of the northeastern South China Sea and surrounding
839 fluvial drainage basins: Source and transport. *Mar. Geol.* 277, 48-60.

- 840 Liu, Z., Trentesaux, A., Clemens, S.C., Colin, C., Wang, P., Huang, B., Boulay, S., 2003. Clay mineral
841 assemblages in the northern South China Sea: implications for East Asian monsoon evolution over the past 2
842 million years. *Mar. Geol.* 201, 133-146.
- 843 Lo, C. H., Onstott, T. C., 1995. Rejuvenation of K-Ar isotope systems for minerals in the Taiwan Mountain Belt.
844 *Earth Planet. Sci. Lett.* 131, 71-98.
- 845 Lock, J., 2007. Interpreting Low-temperature Thermochronometric Data in Fold-and-thrust Belts: An Example
846 from the Western Foothills, Taiwan. University of Washington.
- 847 Lu, C.-Y., Hsü, K.J., 1992. Tectonic evolution of the Taiwan mountain belt. *Petroleum Geology of Taiwan* 27,
848 21-46.
- 849 Lüdmann, T., Kin Wong, H., Wang, P., 2001. Plio–Quaternary sedimentation processes and neotectonics of the
850 northern continental margin of the South China Sea. *Mar. Geol.* 172, 331-358.
- 851 Lundberg, N., Dorsey, R.J., 1990. Rapid Quaternary emergence, uplift, and denudation of the Coastal Range,
852 Eastern Taiwan. *Geology* 18, 638-641.
- 853 Marr, J.G., Swenson, J.B., Paola, C., and Voller, V.R., 2000. A two-diffusion model of fluvial stratigraphy in
854 closed depositional basins: *Basin Research*, v. 12, no. 3-4, p. 381–398.
- 855 Meng, C.-Y., 1967. The structural development of the southern half of western Taiwan. *Proceedings of the*
856 *Geological Society of China* 10, 77-82.
- 857 Métivier, F., Gaudemer, Y., Tapponnier, P., Klein, M., 1999. Mass accumulation rates in Asia during the
858 Cenozoic. *Geophys. J. Int.* 137, 280-318.
- 859 Miller, K.G., Mountain, G.S., Wright, J.D., Browning, J.V., 2011. A 180-Million-Year Record of Sea Level and
860 Ice Volume Variations from Continental Margin and Deep-Sea Isotopic Records. *Oceanography* 24, 40-53.
- 861 Milliman, J.D., Kao, S.-J., 2005. Hyperpycnal discharge of fluvial sediment to the ocean: impact of super-
862 Typhoon Herb (1996) on Taiwanese rivers. *The Journal of Geology* 113, 503-516.
- 863 Milliman, J.D., Lin, S.W., Kao, S.J., Liu, J.P., Liu, C.S., Chiu, J.K., Lin, Y.C., 2007. Short-term changes in
864 seafloor character due to flood-derived hyperpycnal discharge: Typhoon Mindulle, Taiwan, July 2004. *Geology*
865 35, 779-782.
- 866 Milliman, J.D., Syvitski, J.P.M., 1992. Geomorphic/Tectonic Control of Sediment Discharge to the Ocean: The
867 Importance of Small Mountainous Rivers. *J. Geol.* 100, 525-544.
- 868 Mouthereau, F., Lacombe, O., 2006. Inversion of the Paleogene Chinese continental margin and thick-skinned
869 deformation in the Western Foreland of Taiwan. *J. Struct. Geol.* 28, 1977-1993.
- 870 Mouthereau, F., Lacombe, O., Deffontaines, B., Angelier, J., Brusset, S., 2001. Deformation history of the
871 southwestern Taiwan foreland thrust belt: insights from tectono-sedimentary analyses and balanced cross-
872 sections. *Tectonophysics* 333, 293-322.
- 873 Mutti, E., 1977. Distinctive thin-bedded turbidite facies and related depositional environments in the Eocene
874 Hecho Group (South-central Pyrenees, Spain). *Sedimentology* 24, 107-131.
- 875 Naden, P., Broadhurst, P., Tauveron, N., and Walker, A., 1999. River routing at the continental scale: use of
876 globally-available data and an a priori method of parameter estimation: *Hydrology and Earth System Sciences*, v.
877 3, no. 1, p. 109–124.
- 878 Nagel, S., 2012. Sedimentary record of arc-continent collision in Taiwan. PhD Thesis. ETH-Zürich. DISS. ETH
879 NO. 20811
- 880 Nagel, S., Castelltort, S., Wetzel, A., Willett, S.D., Mouthereau, F., Lin, A.T., 2013. Sedimentology and foreland
881 basin paleogeography during Taiwan arc continent collision. *J. Asian Earth Sci.* (10.1016/j.jseaes.2012.09.001).
- 882 Naylor, M., Sinclair, H.D., 2008. Pro- vs. retro-foreland basins. *Basin Res.* 20, 285-303.
- 883 Olariu, C., Steel, R.J., 2009. Influence of point-source sediment-supply on modern shelf-slope morphology:
884 implications for interpretation of ancient shelf margins. *Basin Res.* 21, 484-501.
- 885 Pan, T.-S., 2011. A study on sedimentary environments of Nanchuang Formation to Yangmei Formation along
886 the Dahan River section, northwestern Taiwan, Department of Earth Sciences. National Central University,
887 Jhongli.
- 888 Paola, C., Heller, P.L., and Angevine, C.L., 1992. The large-scale dynamics of grain-size variation in alluvial
889 basins, 1: Theory: *Basin Research*, v. 4, p. 73–90.
- 890 Pelletier, B., Stephan, J.F., 1986. Middle Miocene obduction and late Miocene beginning of collision registered
891 in the Hengchun Peninsula: geodynamic implications for the evolution of Taiwan. *Tectonophysics* 125, 133-160.

- 892 Posamentier, H.W., and Allen, G.P., 1993. Siliciclastic sequence stratigraphic patterns in foreland, ramp-type
893 basins: *Geology*, v. 21, no. 5, p. 455, doi: 10.1130/0091-7613
- 894 Puigdefàbregas, C., and Souquet, P., 1986. Tecto-sedimentary cycles and depositional sequences of the
895 Mesozoic and Tertiary from the Pyrenees: *Tectonophysics*, v. 129, no. 1, p. 173–203.
- 896 Peng, TH., Li, Y.-H., and Wu, F., 1977. Tectonic uplift rates of the Taiwan island since the early Holocene.
897 *Memoir of the Geological Society of Taiwan*, 2, 57-69.
- 898 Puigdefàbregas, C., Muñoz, J.A., Vergés, J., 1992. Thrusting and foreland basin evolution in the southern
899 Pyrenees, in: McClay, K. (Ed.), *Thrust tectonics*. Chapman & Hall, London, pp. 247-254.
- 900 Resentini, A., L. Goren, S. Castellort, and E. Garzanti (2017), Partitioning sediment flux by provenance and
901 tracing erosion patterns in Taiwan, *J. Geophys. Res. Earth Surf.*, 122, doi:10.1002/2016JF004026.
- 902 Rivenaes, J.C., 2007. Application of a dual-lithology, depth-dependent diffusion equation in stratigraphic
903 simulation: *Basin Research*, v. 4, no. 2, p. 133–146, doi: 10.1306/212F926E-2B24-11D7-8648000102C1865D.
- 904 Romans, B.W., Castellort, S., Covault, J.A., Fildani, A., Walsh, J.P., 2016. Environmental signal propagation in
905 sedimentary systems across timescales. *Earth Science Reviews* 153, 7–29. doi:10.1016/j.earscirev.2015.07.012
- 906 Schlager, W., and Adams, E.W., 2001. Model for the sigmoidal curvature of submarine slopes: *Geology*, v. 29,
907 no. 10, p. 883, doi: 10.1130/0091-7613(2001)029<0883:MFTSCO>2.0.CO;2.
- 908 Seno, T., Kawanishi, Y., 2009. Reappraisal of the Arc-Arc Collision in Taiwan. *Terr. Atmos. Ocean Sci.* 20,
909 573-585.
- 910 Seno, T., Stein, S., Grip, A.E., 1993. A model for the motion of the Philippine Sea plate consistent with
911 NUVEL-1 and geologic data. *J. Geophys. Res.* 98 (B10), 941–948.
- 912 Shaw, C.-L., 1996. Stratigraphic correlation and isopach maps of the Western Taiwan Basin. *Terr. Atmos. Ocean*
913 *Sci.* 7, 333-360.
- 914 Siame, L.L., Angelier, J., Chen, R.F., Godard, V., Derrieux, F., Bourlès, D.L., Braucher, R., Chang, K.J., Chu,
915 H.T., Lee, J.C., 2011. Erosion rates in an active orogen (NE-Taiwan): A confrontation of cosmogenic
916 measurements with river suspended loads. *Quat. Geochronol.* 6, 246-260.
- 917 Siame, L.L., Chen, R.-F., Derrieux, F., Lee, J.-C., Chang, K.-J., Bourlès, D.L., Braucher, R., Leanni, L., Kang,
918 C.-C., Chang, C.-P., Chu, H.-T., 2012. Pleistocene alluvial deposits dating along frontal thrust of Changhua Fault
919 in western Taiwan: the cosmic ray exposure point of view. *J. Asian Earth Sciences* 51, 1-20.
- 920 Sibuet, J.-C., Hsu, S.-K., 1997. Geodynamics of the Taiwan arc-arc collision. *Tectonophysics* 274, 221-251.
- 921 Sibuet, J.-C., Hsu, S.-K., 2004. How was Taiwan created? *Tectonophysics* 379, 159-181.
- 922 Sibuet, J.-C., Hsu, S.-K., Shyu, C.-T., Liu, C.S., 1995. Structural and kinematic evolutions of the Okinawa
923 trough backarc basin, in: Taylor, B. (Ed.), *Backarc Basins: Tectonics and Magmatism*. Plenum Press.
- 924 Silver, E.A., Abbott, L.D., Kirchoff-Stein, K.S., Reed, D.L., Bernstein-Taylor, B., Hilyard, D., 1991. Collision
925 propagation in Papua New Guinea and the Solomon Sea. *Tectonics* 10, 863-874.
- 926 Simoes, M., Avouac, J.P., Beyssac, O., Goffé, B., Farley, K.A., Chen, Y.-G., 2007. Mountain building in
927 Taiwan: A thermokinematic model. *J. Geophys. Res.* 112, B11405.
- 928 Simoes, M., Avouac, P., 2006. Investigating the kinematics of mountain building in Taiwan from the
929 spatiotemporal evolution of the foreland basin and western foothills. *J. Geophys. Res.* 11.
- 930 Simpson, G., 2014. Decoupling of foreland basin subsidence from topography linked to faulting and erosion:
931 *Geology*, doi: 10.1130/G35749.1.
- 932 Sinclair, H.D., Coakley, B.J., Allen, P.A., Watts, A.B., 1991. Simulation of foreland basin stratigraphy using a
933 diffusion-model of mountain belt uplift and erosion - an example from the central Alps, Switzerland. *Tectonics*
934 10, 599-620.
- 935 Sinclair, H.D., Naylor, M., 2012. Foreland basin subsidence driven by topographic growth versus plate
936 subduction. *Geol. Soc. Am. Bull.* 124, 368-379.
- 937 Sømme, T.O., Helland-Hansen, W., Martinsen, O.J., Thurmond, J.B., 2009. Relationships between
938 morphological and sedimentological parameters in source-to-sink systems: a basis for predicting semi-
939 quantitative characteristics in subsurface systems. *Basin Res.* 21, 361-387.
- 940 Song, S.-R., Liu, C.-M., Chen, C.-H., Lo, W., 2004. Pumice layers in marine terraces: Implications for tectonic
941 uplift rates on the east and northeast coasts of Taiwan over the last hundreds of years. *Quaternary International*,
942 115-116, 83-92.
- 943 Stolar, D.B., Willett, S.D., Montgomery, D.R., 2007. Characterization of topographic steady state in Taiwan.
944 *Earth Planet. Sci. Lett.* 261, 421-431.

- 945 Su, D., White, N., McKenzie, D.A.N., 1989. Extension and subsidence of the Pearl River Mouth Basin, northern
946 South China Sea. *Basin Res.* 2, 205-222.
- 947 Suppe, J., 1981. Mechanics of mountain-building and metamorphism in Taiwan. *Memoir of the Geological*
948 *Society of China* 4, 67-89.
- 949 Suppe, J., 1984. Kinematics of arc-continent collision, flipping of subduction, and back-arc spreading near
950 Taiwan. *Memoir of the geological society of China* 6, 21-33.
- 951 Suppe, J., 1988. Tectonics of arc-continent collision on both sides of the south China sea: Taiwan and Mindoro.
952 *Acta Geol. Taiwan.* 26, 1-18.
- 953 Teng, L.S., 1990. Geotectonic evolution of late Cenozoic arc-continent collision in Taiwan. *Tectonophysics* 183,
954 57-76.
- 955 Tensi, J., Mouthereau, F., Lacombe, O., 2006. Lithospheric bulge in the West Taiwan Basin. *Basin Res.* 18, 277-
956 299.
- 957 Ting, H.-H., Huang, C.-Y., Wu, L.-C., 1991. Paleoenvironments of the late neogene sequences along the
958 Nantzuhsien river, Southern Taiwan. *Petroleum Geology of Taiwan* 26, 121-149.
- 959 Tropeano, M., Sabato, L., Pieri, P., 2002. Filling and cannibalization of a foredeep: the Bradanic Trough,
960 Southern Italy. *Geological Society, London, Special Publications* 191, 55-79.
- 961 Vergés, J., Burbank, D.W., 1996. Eocene-Oligocene thrusting and basin configuration in the eastern and central
962 Pyrenees (Spain), in: Friend, Dabrio (Eds.), *Tertiary Basins of Spain*, Cambridge University Press ed, pp. 120-
963 133.
- 964 Wan, S., Li, A., Clift, P.D., Jiang, H., 2006. Development of the East Asian summer monsoon: Evidence from
965 the sediment record in the South China Sea since 8.5 Ma. *Palaeogeography, Palaeoclimatology, Palaeoecology*
966 241, 139-159.
- 967 Wang, C.-H., Burnett, W.C., 1990. Holocene mean uplift rates across an active plate collision boundary in
968 Taiwan. *Bulletin Institute of Earth Sciences, Academia Sinica*, 10, 40.
- 969 Wang, H., Yang, Z., Saito, Y., Liu, J.P., Sun, X., Wang, Y., 2007. Stepwise decreases of the Huanghe (Yellow
970 River) sediment load (1950–2005): Impacts of climate change and human activities. *Global Planet. Change* 57,
971 331-354.
- 972 Wang, S., Chen, Z., Smith, D.G., 2005. Anastomosing river system along the subsiding middle Yangtze River
973 basin, southern China. *Catena* 60, 147-163.
- 974 Watts, A.B., Ryan, W.B.F., 1976. Flexure of the lithosphere and continental margin basins. *Tectonophysics* 36,
975 25-44.
- 976 Whipple, K.X., 2001. Fluvial landscape response time: how plausible is steady-state denudation?: *American*
977 *Journal of Science*, v. 301, no. 4-5, p. 313–325.
- 978 White, N.M., Pringle, M., Garzanti, E., Bickle, M., Najman, Y., Chapman, H., Friend, P., 2002. Constraints on
979 the exhumation and erosion of the high Himalayan slab, NW India, from foreland basin deposits. *Earth Planet.*
980 *Sci. Lett.* 195, 29-44.
- 981 Willett, S.D., Brandon, M.T., 2002. On steady state in mountains belts. *Geology* 30, 175-178.
- 982 Willett, S.D., Fisher, D., Fuller, C., En-Chao, Y., Chia-Yu, L., 2003. Erosion rates and orogenic-wedge
983 kinematics in Taiwan inferred from fission-track thermochronometry. *Geology* 31, 945-948.
- 984 Wolanski, E., King, B., Galloway, D., 1995. Dynamics of the turbidity maximum in the Fly River estuary, Papua
985 New Guinea. *Estuar. Coast. Shelf Sci.* 40, 321-337.
- 986 Wu, W.-N., Hsu, S.-K., Lo, C.-L., Chen, H.-W., Ma, K.-F., 2009. Plate convergence at the westernmost
987 Philippine Sea Plate. *Tectonophysics* 466, 162-169.
- 988 Wu, Y.-M., Chang, C.-H., Zhao, L., Shyu, J.B.H., Chen, Y.-G., Sieh, K., Avouac, J.-P., 2007. Seismic
989 tomography of Taiwan: Improved constraints from a dense network of strong motion stations. *J. Geophys. Res.*
990 112, B08312.
- 991 Xiong, P., Shaokun, Y., Ming, Z.H.U., Jinsong, L.I., 2004. Deep-water Fan Systems and Petroleum Resources
992 on the Northern Slope of the South China Sea. *Acta Geologica Sinica - English Edition* 78, 626-631.
- 993 Xu, K., Milliman, J.D., Li, A., Paul Liu, J., Kao, S.-J., Wan, S., 2009. Yangtze- and Taiwan-derived sediments
994 on the inner shelf of East China Sea. *Cont. Shelf Res.* 29, 2240-2256.
- 995 Yamaguchi, M., Ota, Y., 2004. Tectonic interpretations of Holocene marine terraces, east coast of Coastal
996 Range, Taiwan. *Quaternary International* 115-116, 71-81.

- 997 Yang, B.C., Chun, S.S., 2001. A seasonal model of surface sedimentation on the Baeksu open-coast intertidal
998 flat, southwestern coast of Korea. *Geosci. J.* 5, 251-262.
- 999 Yang, T.F., Tien, J.-I., Chen, C.-H., Lee, T., Punongbayan, R.S., 1995. Fission-track dating of volcanics in the
1000 northern part of the Taiwan-Luzon Arc: eruption ages and evidence for crustal contamination. *J. Southeast.*
1001 *Asian Earth Sci.* 11, 81-93.
- 1002 Yeh, M.-G., Chang, Y.-L., 1991. The ichnofacies study of the Ailiaochiao formation, the Changchihkeng
1003 formation, Chiahsien-Meinung area, Kaohsiung. *Petroleum Geology of Taiwan* 26, 151-181.
- 1004 Yeh, M.-G., Yang, C.-Y., 1994. Depositional environments of the upper Miocene to Pleistocene series in the
1005 Chungpu area, Chiayi, Taiwan. *Petroleum Geology of Taiwan* 29, 193-224.
- 1006 Yu, H.-S., Chang, J.-F., 2002. The Penghu Submarine Canyon off Southwestern Taiwan: Morphology and
1007 Origin. *Terr. Atmos. Ocean Sci.* 13, 547-562.
- 1008 Yu, H.-S., Chiang, C.-S., Shen, S.-M., 2009. Tectonically active sediment dispersal system in SW Taiwan
1009 margin with emphasis on the Gaoping (Kaoping) Submarine Canyon. *Journal of Marine Systems* 76, 369-382.
- 1010 Yu, H.-S., Chou, Y.-W., 2001. Characteristics and development of the flexural forebulge and basal unconformity
1011 of western Taiwan foreland Basin. *Tectonophysics* 333, 277-291.
- 1012 Yu, H.-S., Hong, E., 2006. Shifting submarine canyons and development of a foreland basin in SW Taiwan:
1013 controls of foreland sedimentation and longitudinal sediment transport. *J. Asian Earth Sci.* 27, 922-932.
- 1014 Yu, H.-S., Huang, C.-S., Ku, J.-W., 1991. Morphology and possible origin of the Kaoping submarine canyon
1015 head off SW Taiwan. *Acta Geol. Taiwan.* 27, 40-50.
- 1016 Yu, H.-S., Huang, Z.-Y., 2006. Intraslope Basin, Seismic Facies and Sedimentary Processes in the Kaoping
1017 Slope, Offshore Southwestern Taiwan. *Terr. Atmos. Ocean Sci.* 17, 659-677.
- 1018 Yu, H.-S., Huang, Z.-Y., 2009. Morphotectonics and sedimentation in convergent margin basins: An example
1019 from juxtaposed marginal sea basin and foreland basin, Northern South China Sea. *Tectonophysics* 466, 241-
1020 254.
- 1021 Yu, N.-T., Teng, L.S., Chen, W.-S., Yen, I.-C., 2008. Facies characteristics of the upper-Neogene
1022 Nantzuhsienchi Section, Kaohsiung, SW Taiwan. *Petroleum Geology of Taiwan* 38, 30-56.
- 1023 Yu, S.B., Chen, H.Y., Kuo, L.C., 1997. Velocity of GPS stations in the Taiwan area. *Tectonophysics* 274, 41-59.
- 1024 Zhang, S., Lu, X.X., Higgitt, D.L., Chen, C.-T.A., Han, J., Sun, H., 2008. Recent changes of water discharge and
1025 sediment load in the Zhujiang (Pearl River) Basin, China. *Global Planet. Change* 60, 365-380.
- 1026 Zheng, H., Powell, C.M., Rea, D.K., Wang, J., Wang, P., 2004. Late Miocene and mid-Pliocene enhancement of
1027 the East Asian monsoon as viewed from the land and sea. *Global Planet. Change* 41, 147-155.